

## Review

Recent advances in *in-situ* transmission electron microscopy techniques for heterogeneous catalysisJiangshan Qu,<sup>1,2</sup> Manling Sui,<sup>3,\*</sup> and Rengui Li<sup>1,\*</sup>

## SUMMARY

The process of heterogeneous catalytic reaction under working conditions has long been considered a “black box”, which is mainly because of the difficulties in directly characterizing the structural changes of catalysts at the atomic level during catalytic reactions. The development of *in situ* transmission electron microscopy (TEM) techniques offers opportunities for introducing a realistic chemical reaction environment in TEM, making it possible to uncover the mystery of catalytic reactions. In this article, we present a comprehensive overview of the application of *in situ* TEM techniques in heterogeneous catalysis, highlighting its utility for observing gas-solid and liquid-solid reactions during thermal catalysis, electrocatalysis, and photocatalysis. *in situ* TEM has a unique advantage in revealing the complex structural changes of catalysts during chemical reactions. Revealing the real-time dynamic structure during reaction processes is crucial for understanding the intricate relationship between catalyst structure and its catalytic performance. Finally, we present a perspective on the future challenges and opportunities of *in situ* TEM in heterogeneous catalysis.

## INTRODUCTION

Heterogeneous catalysis not only contributes significantly to enabling the production of indispensable commodities such as fuels and fertilizer, but also shows great promise in dealing with severe environmental problems.<sup>1–6</sup> The catalytic activity and selectivity definitely depend on the microstructure of catalysts, including the surface structures, interfaces and specific reactive sites.<sup>7,8</sup> Therefore, atomically revealing the microstructures of catalysts under real working conditions is of great significance. Although conventional TEM provides some insights into the atomic structure of catalysts, the heterogeneous catalysis process is always deduced by *ex situ* characterizations before and after catalytic reactions,<sup>9</sup> which sometimes results in vague or even misleading knowledge of the intrinsic mechanism. Studies have shown that the intrinsic physicochemical properties of heterogeneous catalysts under real working conditions often deviate greatly from *ex situ* characterizations.<sup>10,11</sup> The surface structure of catalysts always changes with the adsorption, activation and desorption of the reactant molecules.<sup>12,13</sup> But these microscopic structural changes cannot be sufficiently examined by conventional TEM, making the heterogeneous catalytic reactions like a “black box” (Figure 1). To attain comprehensive knowledge of the intrinsic mechanism of catalytic reactions, an insightful understanding of the physicochemical properties of the catalysts and rationalization of the catalytic structure-activity relationship under realistic reaction conditions are strongly desired.

Because the first electron microscope was constructed by Knoll and Ruska in 1932, its development has never stopped and the spatial resolution keeps improving.<sup>14</sup> Now it is no longer desirable to improve resolution simply by increasing the acceleration voltage to reduce the electron wavelength, because the point resolution is still limited by the spherical aberration of its objective lens; meanwhile, the high-energy electron beam usually causes irreversible damage to the sample.<sup>15,16</sup> The most noteworthy achievement is the successful implantation of aberration correctors in TEM, which makes up for the defects of uneven focus of electromagnetic lenses, resulting in great improvement in spatial resolution even under low voltage conditions.<sup>17,18</sup> In the parallel-illumination TEM mode, the electron beams traverse through the sample and are detected on the opposite side. The use of parallel illumination is crucial for obtaining sharp selected-area diffraction patterns and optimal classical image contrast. The TEM mode is well-suited for crystal orientation analysis<sup>19</sup> and periodic structure analysis of nanomaterials. In addition, diffraction patterns obtained from TEM mode can provide valuable insights into the crystal structure of the sample. High-resolution

<sup>1</sup>State Key Laboratory of Catalysis, Dalian Institute of Chemical Physics, Chinese Academy of Sciences, Dalian National Laboratory for Clean Energy, The Collaborative Innovation Center of Chemistry for Energy Materials (iChem-2011), Dalian 116023, China

<sup>2</sup>Center of Materials Science and Optoelectronics Engineering, University of Chinese Academy of Sciences, Beijing 100049, China

<sup>3</sup>Beijing Key Laboratory of Microstructure and Properties of Solids, Faculty of Materials and Manufacturing, Beijing University of Technology, Beijing 100124, China

\*Correspondence: mlsui@bjut.edu.cn (M.S.), rgli@dicp.ac.cn (R.L.)

<https://doi.org/10.1016/j.isci.2023.107072>



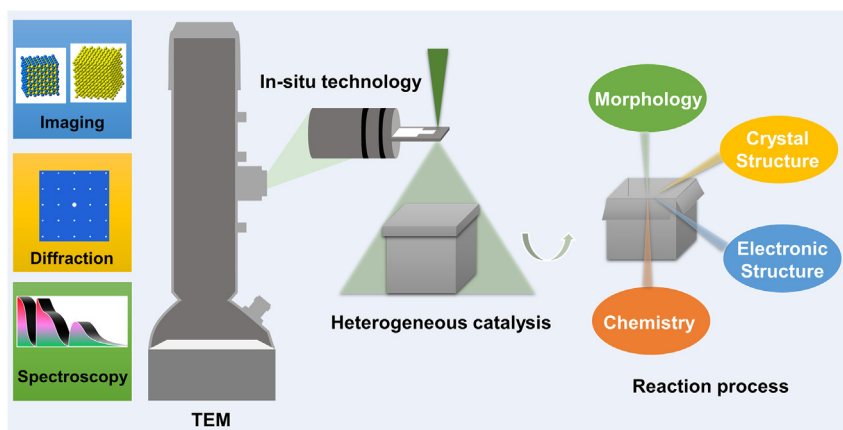


**Figure 1. Overview of the important role of *in situ* TEM in heterogeneous catalysis**

TEM enables the observation of interfacial structure analysis,<sup>20</sup> and fine structures including dislocations and twins,<sup>21</sup> and coherent boundary.<sup>22</sup>

In addition, scanning TEM (STEM) was developed by Ardenne in 1938.<sup>23–25</sup> In STEM mode, the electron beam is focused into a small spot and scanned across the sample, thereby generating a high-resolution image through the collection of scattered electrons produced by the interaction between the beam and sample. The high-angle annular dark field (HAADF) image exhibits atomic number sensitivity while being insensitive to sample thickness and electron microscope focusing changes. Furthermore, the implementation of spherical aberration correctors facilitates achieving sub-angstrom resolution levels. Therefore, utilizing HAADF mode provides an advantage in imaging single-atom catalysts<sup>8</sup> by enhancing the visibility of heavy atoms. Equipped with energy dispersive X-ray spectroscopy (EDS)<sup>26,27</sup> and electron energy loss spectroscopy (EELS),<sup>28–30</sup> STEM can provide comprehensive information on morphology, crystal structure, chemical composition, and electronic structure of catalysts with atomic resolution.<sup>31–33</sup>

Heterogeneous catalytic reactions are commonly conducted under gas-solid or liquid-solid conditions, so it is necessary to introduce gas or liquid reactants into TEM to approach the realistic catalytic reaction condition. Environmental TEM (ETEM) is a specially modified TEM, which allows gas reactants into the sample chamber while maintaining the main column at a high vacuum by pressure-limiting apertures.<sup>34–39</sup> Moreover, various sample holders have been designed to cross the pressure gap based on micro-electromechanical system (MEMS) technology,<sup>40,41</sup> which allow the catalyst to make direct contact with the reactant molecules in the sealed cell.<sup>42–44</sup> Besides gas and liquid environments, the integration of other excitation conditions for catalytic reactions can also be achieved in TEM, such as thermal,<sup>45,46</sup> electrical,<sup>47–49</sup> mechanical<sup>50</sup> and optical excitation.<sup>51</sup>

Herein, we briefly review the developments of *in situ* TEM techniques and their recent advances in heterogeneous catalysis. *in situ* TEM possesses a unique advantage in elucidating the structural transformations of catalysts during reactions. It is of paramount importance to unveil the real-time dynamic structure during reaction processes, thereby unraveling the mechanism of catalytic reactions and establishing the correlation between structure and performance.

### ***In situ* TEM technologies for gas and liquid phase**

The key challenge of directly observing dynamic changes of catalysts under operation conditions is to overcome the pressure gap between realistic reaction conditions and the pressure of simulated reactions in the TEM. For TEM, the electron gun and electron beam path must be kept in a high vacuum to reduce scattering of the electron beam, thus keeping the coherence of the electron beam to get high-quality images. Two approaches have been developed to introduce gas or liquid into the TEM: One is the differential pumping system (Figure 2A),<sup>39</sup> which separates the specimen chamber from the main column by using pressure-limiting apertures; the other is the specimen holders (Figure 2B),<sup>52,53</sup> which enclose the catalyst and gas or liquid within a sealed cell by window membranes transparent to the electron beam.

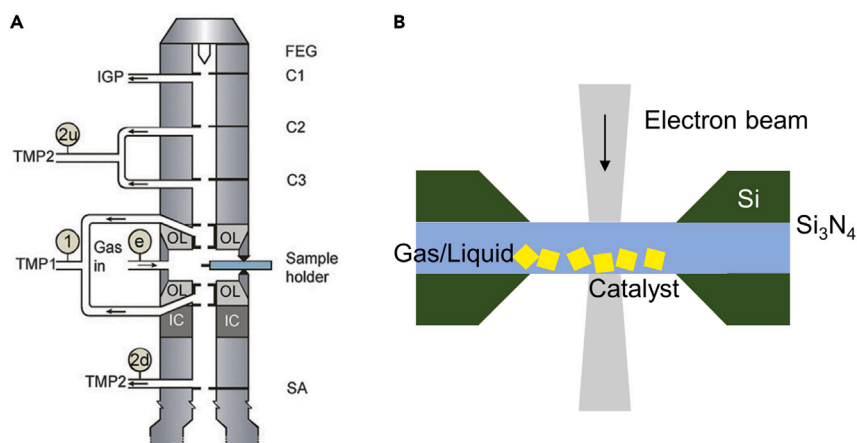


**Figure 2. The schematic illustration of a differential pumping system and a liquid cell**

(A) The schematic illustration of an ETEM equipped with pressure-limiting apertures and a differential pumping system. Adapted with permission.<sup>39</sup> Copyright 2012, Elsevier Ltd.

(B) The schematic illustration of a liquid cell in specimen holders.

### Differential pumping system and aperture

Early in 1942, Ruska<sup>54</sup> tried to separate the TEM column into independently pumped compartments by inserting apertures in the pole piece. Later, Hashimoto et al.<sup>55</sup> constructed a specimen chamber with gas pressure up to 300 Torr from the initial  $10^{-2}$  Torr for high-temperature gas reaction. Then the differential pumping system which allows large pressure differences between the reaction chamber and other vacuum parts has been developed for decades,<sup>37,56</sup> which has been successfully exploited on commercial ETEMs.<sup>34,42</sup> The specimen chamber, where chemical reactions take place, is separated from the main column by the pressure-limiting apertures, as shown in Figure 2A. And the differential pumping system prevents the diffusion of gas molecules from the specimen chamber to other parts of TEM, thus forming different gas pressure between different compartments. Therefore, the gas can be introduced into the sample chamber for chemical reactions without affecting the other parts of TEM. In addition to gases, water vapor can also be introduced into the sample chamber.<sup>57</sup>

### Sealed cell specimen holder

Unlike modified ETEM fitting out with differential pumping systems and apertures, commercial specimen holders are well-compatible with the conventional TEM. There is a sealed cell constructed on the sample holder to encapsulate gas or liquid reactants to avoid leaking to other parts of TEM. Early sealed cells were based on specimen grids.<sup>58–60</sup> Then the development of MEMS technology set off a boom in MEMS-based sealed cells.<sup>61–63</sup> Williamson et al.<sup>64</sup> reported a liquid cell with silicon wafer packaging and a silicon nitride thin film window in 2003. Later, silicon wafers with a silicon nitride membrane window have been developed as the most popular sealing material because of their high strength and excellent electron beam transmission. To reduce the scattering of the electron beam and improve the resolution, the thickness of the silicon nitride membrane and liquid layer sealed in the cell has been decreasing. Current silicon nitride films can be processed to 25 nm or thinner. But the strength requirement limits the further reduction in thickness because the films need to be strong enough to withstand the pressure difference across the films. The liquid layer thickness can be limited to 100 nm by adding a sticky metal layer of indium between the upper and lower silicon wafers,<sup>65</sup> or be further reduced without any interlayer.<sup>52</sup> Also the liquid can be injected through a peristaltic pump, and the flow rate can be adjusted flexibly.<sup>52</sup> But some studies have shown that silicon nitride films usually bend because of the large pressure difference between the high vacuum in TEM and the liquid environment, so the actual liquid layer is thicker than estimated.<sup>66,67</sup> To solve this problem, the pressure control system was introduced.<sup>66,68</sup> In addition, other alternative encapsulation materials such as graphene are also under exploration, of which graphene received wide attention because of its unique advantages, thin, strong, and impervious to water.<sup>69,70</sup> Compared to other liquid cells, graphene cell allows observation of catalysts in liquid environments with minimal contrast and resolution loss.<sup>71,72</sup> Now the behavior of single adatoms in liquid can be tracked in TEM by using graphene liquid cells.<sup>73</sup>

Here, we conduct a systematic comparison of the advantages and disadvantages between ETEM and gas cells, MEMS cells and graphene cells, respectively. In ETEM, high resolution can be achieved because of the absence of a sealed window material that may scatter the electron beam and the low pressure of the gas that can pass through. In some studies, the adsorbed species on highly ordered surface sites can be imaged,<sup>57,74</sup> laying the foundation to explore the catalytic reaction processes atomically. However, the pressure of gas allowed in the sample chamber remains below atmospheric pressure, typically below 15 Torr.<sup>75,76</sup> It is worth noting that catalyst behavior under such low-pressure conditions may deviate from realistic reaction conditions. Gas cells with windows provide a distinct gas environment that is isolated from other parts of the TEM column, where higher pressure limits are present. This unique setup allows researchers to investigate the behavior of catalysts under operational conditions, which is particularly advantageous. In addition, gas cells offer superior control over the reaction process and come at a much lower cost than dedicated ETEM systems that utilize differential-pumping approaches. The early development of MEMS technology has led to the commercialization of numerous MEMS cells. Currently, MEMS cells can be utilized to facilitate the passage of not only gas and liquid but also heat, electricity, and light, which have found applications in various fields such as thermal catalysis, electrocatalysis, and emerging photocatalytic reactions. However, the typical encapsulation of liquid in MEMS cells requires a double layer of silicon nitride films, which can lead to electron beam scattering and limits the achievable resolution to a few nanometres.<sup>65,77</sup> In contrast, graphene cells employ graphene layers for encapsulating liquid, resulting in minimal electron beam scattering and enabling atomic-level resolution.<sup>73</sup> Despite this advantage, the practical implementation of graphene cells is still limited to laboratory settings. Early graphene liquid cells relied on the random formation of liquid pockets between two graphene sheets,<sup>70</sup> whose location and dimensions are not predictable. These randomly formed liquid pockets are of poor repeatability and poor stability under electron beam irradiation. The subsequent introduction of patterned spacer layers of SiNx or hexagonal boron nitride allowed the position and size of the liquid pockets to be controlled.<sup>78,79</sup> However, the integration of liquid flow and electrical bias has not yet been achieved. In addition, it is important to distinguish the movements in liquid when imaging or the electron-beam effects on a dried sample under or on graphene.<sup>80</sup>

### **In situ TEMs in heterogeneous catalysis**

Heterogeneous catalytic reactions are commonly conducted in gas-solid or liquid-solid environments, which are considered to be the process of adsorption, reaction and desorption of reactant molecules on the surface of the catalyst.<sup>81,82</sup> But we know little about the structural changes of the catalysts during reactants' adsorption and reactivation, although these are of significance to understanding the reaction mechanism. *in situ* TEM provides direct insight into the structural evolution of catalysts during the reaction. In addition to crystallographic structure, dynamic information on chemical composition and electronic structure can also be obtained. EDS is commonly employed to scrutinize the elemental identity and content of microcomponents in materials. This method leverages the generation of characteristic X-rays during the interaction of the electron beam with substances to provide insights into the chemical composition of samples. EDS is suitable for qualitative and semi-quantitative detection of a vast majority of elements.<sup>83</sup> EELS is capable of uncovering rich information on the electron state at the atomic level across a diverse range of materials, including the elemental types, as well as their valence and concentration distributions and the structure-related atom radial distribution.<sup>84,85</sup>

### **Gas-solid catalytic reaction**

The gas-solid catalytic reaction is one of the most widely used and largest-scale reaction processes in the chemical industry. The earliest industrial gas-solid catalytic reaction goes back to the oxidation of sulfur dioxide to sulfur trioxide on the solid Pt catalyst in 1832.<sup>86</sup> At present, many important industrial reaction processes, such as CO oxidation and ammonia synthesis,<sup>87</sup> catalytic cracking and catalytic reforming in petroleum refining<sup>88</sup> fall into this category.

Gas-solid catalytic reactions usually take place at the surface of the solid catalysts.<sup>89–91</sup> The process of adsorption, activation and desorption of gas molecules on solid catalysts is complex with continuous formation and breaking of chemical bonds, as well as energy exchange and electron transfer, which will also induce structural changes in solid catalysts, including surface reconstruction, morphology evolution, crystal phase transition and so on. Furthermore, the combination of TEM and residual gas analysis mass spectrometry enables simultaneous observation of catalyst structure changes and tracking of gas composition changes.<sup>92</sup> This allows for the establishment of a correlation between catalyst structure and activity during reaction processes.

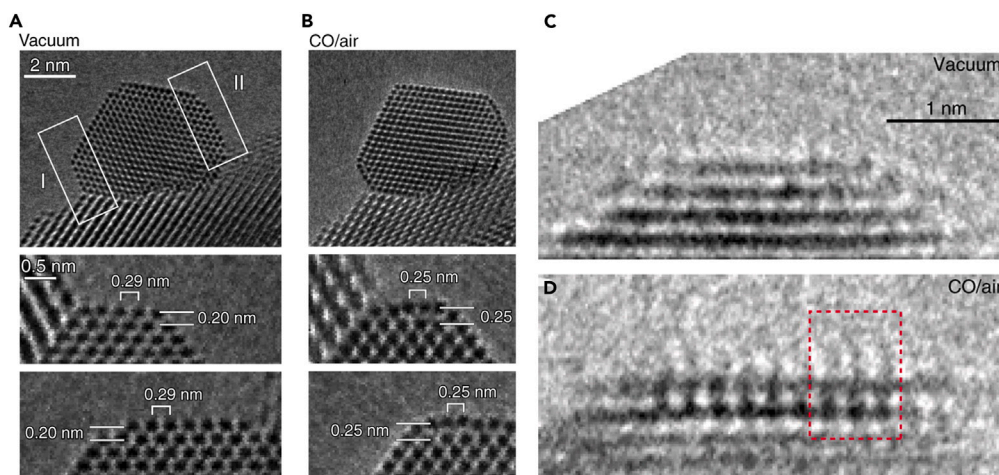


**Figure 3. HRTEM images of Au nanoparticles supported on CeO<sub>2</sub> in different environments**

(A) Au/CeO<sub>2</sub> in vacuum conditions.

(B) Au/CeO<sub>2</sub> in reaction conditions (1 vol % CO in air gas, 45 Pa at room temperature).

(C) Reconstructed surface of Au nanoparticles in vacuum conditions.

(D) Reconstructed surface of Au nanoparticles in reaction condition (1 vol % CO in air gas, 100 Pa at room temperature).

Adapted with permission.<sup>74</sup> Copyright 2012, American Association for the Advancement of Science.

### Surface reconstruction

The adsorption and activation of gas molecules on solid catalysts may break the equilibrium state of the surface atoms. For instance, the surface restructures of Au nanoparticles supported on CeO<sub>2</sub> during CO oxidation were revealed by Yoshida and Takeda et al. utilizing ETEM.<sup>74</sup> It is found that the distance between Au atoms on the surface layer and the spacing between surface and subsurface layers changed during the reaction. The distance between Au atomic columns on {100} surface changed from 0.29 nm to 0.25 nm, and spacing between surface and subsurface layers increased from 0.20 nm to 0.25 nm (Figures 3A and 3B). Moreover, the adsorbed CO molecules were observed on the surface Au atoms at restructured {100} facets (Figures 3C and 3D). This identifiable atomic movement indicates the surface reconfiguration of the catalyst caused by the adsorption of the reactants.

Moreover, the surface reconstruction process caused by the adsorption of reactant molecules is also different for catalysts with different physical structures. It is proved that the Ni-Au core-shell nanoparticles show element redistribution under CO<sub>2</sub> hydrogenation reactions.<sup>93</sup> The Ni-Au catalyst is typically a core-shell structure with an ultrathin Au shell covering the Ni core before and after the reaction. However, ETEM results show that the Au shell vanished and formed NiAu alloy with the temperature increase in a reactive atmosphere. The reconstructed NiAu alloy surface may be the real reason for highly selective CO production, rather than the core-shell structure (Figure 4). As the temperature reduced, the Au shell reappeared at the outmost surface. The reversible reconstruction is hardly visualized by *ex situ* characterizations before or after the reaction, which overturns the conventional knowledge and urges us to reconsider the catalytic mechanism beyond the stationary model.

### Shape evolution

The selective adsorption of reactant molecules may induce atomic movement and specific crystal facets exposed, thus changing the morphology of the catalyst.<sup>94,95</sup> Revealing the realistic shape evolution of catalysts during the reaction is helpful for us to construct a dynamic model of the catalyst with environmental changes, making up for the deficiency of deducing the reaction mechanism based on the static model.

Hansen et al.<sup>96</sup> revealed that the shape of Cu nanoparticles supported on ZnO changed with the environment encountered. The Cu nanoparticles obtained by reduction of the CuO precursor in pure H<sub>2</sub> were exposed with (111), (110) and (100) facets, as shown in Figures 5A and 5D. Yet, the proportion of (110) and (100) faces exposed on the surface increased obviously when adding H<sub>2</sub>O to H<sub>2</sub>, resulting in a rounder

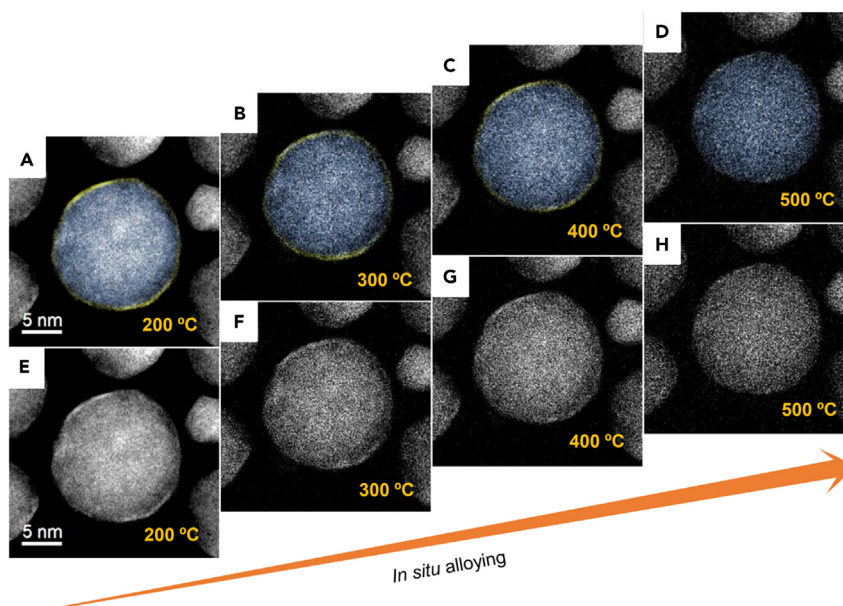


**Figure 4. Structure evolution of a NiAu nanoparticle during CO<sub>2</sub> hydrogenation at elevated temperatures (25 vol % CO<sub>2</sub> and 75 vol % H<sub>2</sub>, 9 mbar)**

(A–D) False colored images of a NiAu nanoparticle at different temperatures. As the temperature rises, the Au-rich shell (highlighted in yellow) gradually disappears.

(E–H) Corresponding high-angle annular dark field (HAADF) images. Adapted with permission.<sup>93</sup> Copyright 2020, Nature Publishing Group.

shape (Figures 5B and 5E). This indicates that H<sub>2</sub>O adsorption induced surface reconstruction and caused shape evolution of Cu nanoparticles. When adding CO to H<sub>2</sub>, Cu nanoparticles transferred into disc-like structures (Figures 5C and 5F). The interface area between Cu and ZnO increased, suggesting that the interface energy was changed by the adsorption of CO. The morphologic evolution of catalysts in different environments has been confirmed under a variety of catalysts, such as PdCu nanocrystals,<sup>97</sup> Pd nanocrystals supported on TiO<sub>2</sub>,<sup>98</sup> Pt nanocrystals supported on SrTiO<sub>3</sub>.<sup>45</sup> Uchiyama and Takeda et al.<sup>99</sup> studied the shape evolution of Au nanoparticles supported on CeO<sub>2</sub> during CO oxidation and established a morphology diagram for the Au/CeO<sub>2</sub> catalyst, which illustrates the dependence between morphology and gas environment.

Moreover, the sensitive response of the interface between metal and substrate to the changes in the external environment will affect the behavior of the metal or substrate. Yuan and Wang et al.<sup>100</sup> reported that the interface structure between Au and TiO<sub>2</sub> could be manipulated by regulating the gas environment. The experiments were performed in an ETEM equipped with a heating holder. The atomic steps interface between TiO<sub>2</sub> (001) and Au (111) facets (Figure 6A) became atomically smooth and formed a semi-coherent interface (Figure 6B) as the O<sub>2</sub> pressure increased, which shows the sensitivity and controllability of the interface structure. Besides, Au nanoparticles rotate epitaxially when adding CO into O<sub>2</sub> for fact that the two-dimensional lattice fringes on Au nanoparticles disappeared (Figure 6C). Theoretical calculations explained that the rotation was owing to the change of O<sub>2</sub> adsorption coverage at the perimeter interface. This study breaks with the conventional understanding that the epitaxial interface is rigid and gives the inspiration to manipulate the active interface between metal catalysts and supports by regulating the atmosphere and achieving the coveted goal of precise regulation of chemical reactions.

In addition, the strong metal-support interaction (SMSI) also plays an important role in heterogeneous catalysis. SMSI was originally used to describe the phenomenon that the metal loaded on the substrate shows dramatically suppressed CO and H<sub>2</sub> adsorption after high-temperature reduction treatment. Later, it was found by *in situ* TEM that the substrate would migrate to the metal and form a coating in the high-temperature reduction atmosphere. It is discovered that SMSI occurs not only in the reductive

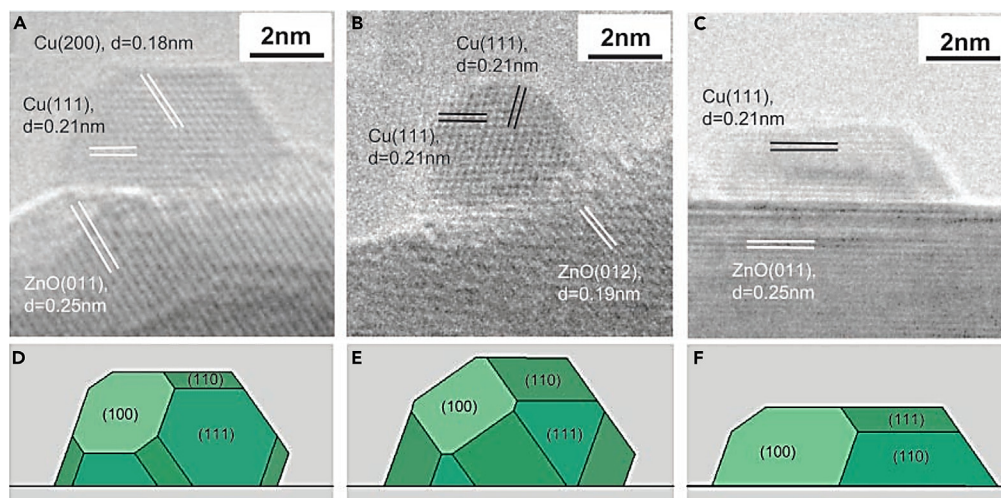


**Figure 5. HRTEM images of Cu nanocrystals supported on ZnO in different environments**

(A)  $\text{H}_2$ , 1.5 mbar, 220°C.

(B)  $\text{H}_2$ :  $\text{H}_2\text{O}$  = 3:1, 1.5 mbar, 220°C.

(C) 95 vol %  $\text{H}_2$  and 5 vol %  $\text{CO}$ , 5 mbar, 220°C.

(D–F) The corresponding Wulff constructions of the Cu nanocrystals. Adapted with permission.<sup>96</sup> Copyright 2002, American Association for the Advancement of Science.

atmosphere, but also in the oxygen atmosphere, and it will disappear when the system is exposed to a redox-reactive environment containing both  $\text{H}_2$  and  $\text{O}_2$ .<sup>101</sup> The experiments were conducted using an *in situ* TEM equipped with a gas cell and a quadrupole mass spectrometer. Once the coating layer on the metal surface disappears, the Pt nanoparticles on the  $\text{TiO}_2$  support become active, whereas their movement modes show crystal orientation dependence (Figure 7). Pt nanoparticles with (111) planes perpendicular to the interface shear up and down along the (111) planes as well as rotate slightly, which is similar to the rotation of Au on  $\text{TiO}_2$  as reported.<sup>100</sup> When the (111) planes parallel to the interface, Pt nanoparticles exhibit a repetitive forward and backward step flow-like motion. Besides, obvious shape evolution was observed when Pt {001} plane parallel to the interface. But when exposed to a reducing atmosphere, the Pt nanoparticles stop movement and the SMSI state is re-established. This study reveals the change of the catalyst from a stable SMSI state to a reactive state in different chemical environments, as well as the crystal orientation-dependent motion behavior in the reactive condition, and complements the understanding of the conditions for the formation and loss of SMSI.

### Adsorption of gas molecular

The ultimate goal to reveal the process of reactants adsorption, dissociating and product desorption on the active sites of the catalyst, thus opening the “black box” of catalytic reaction is challenging. The dynamic change of the catalyst in the chemical reaction makes it difficult to identify the reactive sites. In addition, tracing the real behavior of the reactant molecules during the catalytic reaction is difficult because of the insufficient contrast of single-adsorbed molecules<sup>102,103</sup> and temporal resolution limitations by conventional TEMs.<sup>104</sup>

Yuan and Wang et al.<sup>57,105</sup> devised an ingenious experiment to visualize adsorbed  $\text{H}_2\text{O}$  molecules at the highly ordered surface sites  $\text{TiO}_2$ . They selected  $\text{TiO}_2$  nanocrystals with exposed (001) surface, explored the reconstruction behavior of (001) surface at high temperature, and obtained a stable reconstructed  $\text{TiO}_2$  (001) ( $1 \times 4$ ) surface, which features the highly ordered four-coordinated Ti ( $\text{Ti}_{4c}$ ) rows.<sup>105</sup> Then water vapor was introduced and adsorbed on the top of the  $\text{Ti}_{4c}$  rows in the form of a twin-protrusion configuration (Figure 8).<sup>57</sup> The regular arrangement of  $\text{Ti}_4$  sites along the row direction enhances the contrast of adsorbed  $\text{H}_2\text{O}$  species. The experiments were conducted using an ETEM equipped with a heating holder. This work demonstrates that it is possible to observe the adsorbed species on highly ordered surface sites, one step closer to opening the “black box” of catalytic reaction.

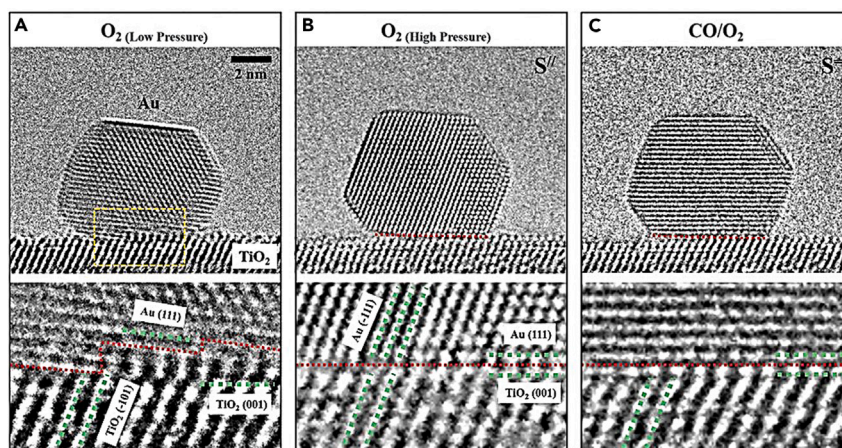


**Figure 6. HRTEM images of an Au nanoparticle supported on TiO<sub>2</sub> (001) surface in different environments**

(A) O<sub>2</sub>, 10<sup>-3</sup> mbar (low-pressure oxygen environment).

(B) O<sub>2</sub>, 6.5 mbar (high-pressure oxygen environment).

(C) 67 vol % CO and 33 vol % O<sub>2</sub>, 4.4 mbar (CO oxidation environment).

Adapted with permission.<sup>100</sup> Copyright 2021, American Association for the Advancement of Science.

### Gas product analysis

The dynamical architecture of a catalyst dictates the accessibility of active sites on its surface. Nevertheless, the mechanisms underlying nanoparticle catalyst restructuring during reaction conditions and their correlation with catalytic activity remain inadequately understood. To establish the correlation between catalyst structure and activity, it is essential to analyze gas products while observing structural changes of catalysts during reactions.<sup>106–108</sup> *in situ* techniques in TEM for measuring gas composition have rapidly developed, including EELS and residual gas analysis (RGA).<sup>92</sup> Both methods offer distinct advantages. EELS techniques provide precise quantitative data and directly analyze the gas within the environmental cell, whereas mass spectrometry utilizing RGA can continuously gather data throughout the experiment.

To observe the oscillatory dynamics of Pt nanoparticles during CO oxidation, Vendelbo et al.<sup>109</sup> utilized a specially designed nanoreactor in TEM to simultaneously monitor structural transformations in Pt particles and changes in gas composition through a combination of mass spectrometry and calorimetry. Mass spectrometry reveals periodic oscillations in O<sub>2</sub> and CO pressures (Figure 9), accompanied by concomitant changes in the morphology of Pt particles (Figure 9B). As the CO conversion increases rapidly, Pt nanoparticles undergo a gradual transformation from a more spherical to a more faceted shape. With a decrease in CO conversion, the nanoparticle reverts to its original spherical shape and maintains this form until another steep rise in CO conversion occurs. This study simultaneously provides atomic-scale information on the surface structure and reactivity of nanoparticles under relevant reaction conditions.

Chee et al.<sup>110</sup> also tracked the morphological changes of noble metal catalysts (Pd, Pt, and Rh) during CO oxidation by TEM within a MEMS gas cell with an integrated thin-film heater, whereas monitoring their catalytic conversion with inline mass spectrometry. The Pd nanoparticles exhibit flat low-index facets and remain inactive toward CO oxidation below 400°C, but undergo a structural transformation resulting in rounder shapes and significantly enhanced CO to CO<sub>2</sub> conversion rates above 400°C (Figures 9C and 9D). In contrast, Pt and Rh nanoparticles do not display such reversible transformations under similar conditions. Subsequently, Ghosh et al.<sup>111</sup> provided further evidence that Pd nanoparticles undergo periodic transitions from a round to a flat shape. The high-index facets of these nanoparticles exhibit periodic emergence and disappearance, coinciding with the transition from high-activity to low-activity states that drive oscillations in reactivity (Figures 9E–9G). This phenomenon is attributed to differences in CO coverage and subsequent modification of surface energy on different facets. Contrary to prevailing beliefs that oscillations only occur under O<sub>2</sub>-rich conditions, they have observed oscillations even in CO-rich environments. Insights into the dynamic surface properties of nanoparticles at an atomic scale under reactive conditions are crucial for the development of efficient catalysts.

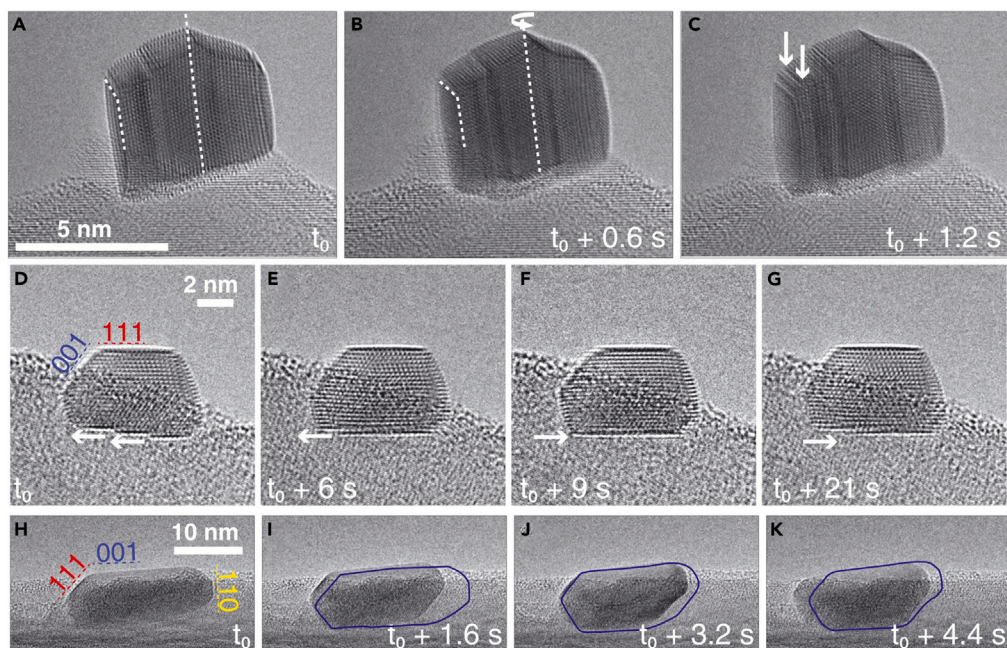


**Figure 7. Crystal orientation-dependent dynamics behavior of Pt nanoparticles on the TiO<sub>2</sub> support in the reactive condition**

(A–C) Pt nanoparticles with (111) planes perpendicular to the interface.

(D–G) Pt nanoparticles with (111) planes parallel to the interface.

(H–K) Pt nanoparticles with {001} plane parallel to the interface.

Adapted with permission.<sup>101</sup> Copyright 2022, American Association for the Advancement of Science.

### Liquid-solid catalytic reaction

Liquid-solid catalysis, like gas-solid catalysis, is also an important field of heterogeneous catalysis, showing fascinating prospects in environmental science, such as electrocatalytic water oxidation<sup>112</sup> and photocatalytic water splitting.<sup>113</sup> The solid-liquid reaction in the TEM usually requires a sealed cell which allows the liquid solution to flow through the TEM, and the solid catalyst is immersed in the flowing liquid. The spatial resolution in TEM of liquids depends on the thickness, stability and beam sensitivity of the samples, of which the number of incident electrons that the sample can tolerate without damage is a key factor in determining image resolution.<sup>65</sup> A series of achievements have been made in exploring crystal nucleation growth<sup>73,114–116</sup> and morphology evolution<sup>117</sup> using liquid cell TEM. Besides, the development of materials science and MEMS has enabled the application of an external potential in a liquid cell to investigate the structural evolution and aging process of electrocatalysts.<sup>118,119</sup> Such an approach can unveil the intricate correlation between catalyst structure and its electrocatalytic performance.

### Surface wettability regulation

The wetting behavior of solid surfaces influenced by an external potential is of paramount importance in heterogeneous catalysis.<sup>120</sup> The hydrophilicity of surfaces has been demonstrated to boost the rate of charge transfer at the electrode-electrolyte interface, thereby enhancing the oxygen evolution reaction (OER) activity.<sup>121</sup> Tileli et al. conducted *in situ* TEM experiments in liquid cells to investigate the dynamic wetting behavior of cobalt-based oxide catalysts for OER under potential cycling.<sup>122</sup> Bright-field images (Figure 10A) were obtained by applying cyclic voltammetry cycles, during the experiment in an alkaline electrolyte solution. The acquired images have revealed a reversible phenomenon of the formation and subsequent dissolution of a dense cloud surrounding the particles, which is observed to be associated with potential cycling (Figure 10B). The potential-dependent contrast variation observed in the images is indicative of the movement of the surrounding alkaline solution and is associated with the modification of the wettability of oxide surfaces (Figure 10C). At low potentials, the oxides exhibited an overall reduction in hydrophobicity. Electrowetting induced a change in interfacial capacitance through reversible reconstruction toward the surface oxyhydroxide phase. At high potentials, the evolution of molecular oxygen was confirmed by operando EELS, and a thinner

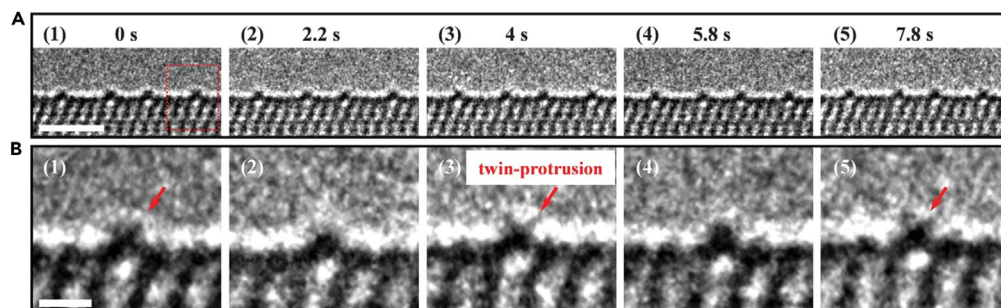


**Figure 8. HRTEM images of absorbed H<sub>2</sub>O on protruded Ti<sub>4c</sub> rows on the TiO<sub>2</sub> (1 × 4) - (001) surface**

(A) Sequential TEM images show the reaction of absorbed H<sub>2</sub>O on protruded Ti<sub>4c</sub> rows.

(B) Corresponding enlarged TEM images of (A).

Adapted with permission.<sup>57</sup> Copyright 2020, American Association for the Advancement of Science.

liquid layer was observed globally. This work establishes a direct relationship between physical wetting and the chemical oxygen evolution reaction of single particles.

### Activation and degradation

To design catalysts that are effective and stable for energy conversion applications, it is important to understand how they transform under reaction conditions and the underlying structure-property relationships. The electrochemical liquid cell TEM allows us to observe changes in the structure of nanocatalysts, monitor particle motion and coalescence, and investigate the dissolution and redeposition processes under working conditions by correlating applied electrochemical potential with the microstructural response. Beermann et al.<sup>123</sup> utilized an *in situ* STEM electrochemical liquid cell to investigate the degradation mechanisms of a carbon-supported Pt-Ni alloy catalyst during cycling reactions. During catalyst activation, they observed the dynamic reaction of a selective Ni dissolution process. The Ni-rich particles became spongy before completely dissolving, and this occurred promptly after some electrochemical cycles rather than constantly. In addition, Pt redeposition at high potential led to the rapid obscuring of the octahedral shape. The catalyst structure underwent the most severe changes during potential cycling and holds. In addition, Peña et al.<sup>123</sup> investigated the structural evolution of Co<sub>3</sub>O<sub>4</sub> nanoparticles during the OER using *in situ* TEM electrochemical liquid cells. They observed a gradual and irreversible amorphization of Co<sub>3</sub>O<sub>4</sub> nanoparticles during water oxidation, which was found to enhance their electrocatalytic activity for water oxidation.

To develop an effective and stable catalyst for CO<sub>2</sub> electroreduction, a series of experiments were conducted by Chee and Cuenya et al. to investigate the electrochemical synthesis and transformation of cubic copper catalysts during the process using a liquid electrochemistry TEM holder.<sup>124–126</sup> Copper oxide cubes were selectively synthesized by adding chloride ions and adjusting the potentials within a narrow range where non-cubic particles dissolve whereas cubic ones remain stable. Figure 11A shows that the particles grew gradually as the potential decreased, however, the electrochemically deposited particles exhibited uneven shape and size distribution. On increasing the potential again, only cubic particles remained on the working electrode while non-cubic structures dissolved. Eventually, even the cubes dissolved as the potential approached 0.20 V. It was subsequently discovered that cubic Cu<sub>2</sub>O catalysts undergo a restructuring process during CO<sub>2</sub> reduction reaction, transforming from a single crystal to a porous and fragmented nanostructure (Figure 11B). Moreover, the leached Cu from the Cu<sub>2</sub>O cubes forms small randomly shaped nanoparticles. The selectivity of C<sub>2+</sub> hydrocarbons is influenced by both the size and surface coverage of cubic catalysts and smaller nanoparticles. Considering that copper is highly sensitive to changes in the presence of halides, they also provided a detailed explanation of how Cu islands undergo restructuring when exposed to iodide before and during CO<sub>2</sub> reduction reaction (Figure 11C). It was found that pre-treating with iodide can enhance the selectivity of hexagonally ordered Cu-island arrays toward ethylene and oxygenate products. These studies have enhanced our understanding of the true nature of catalysts in the reaction process, and provided valuable insights for elucidating the structure-activity relationship and designing more efficient and stable catalysts.

### Light-induced gas/liquid-solid catalytic reaction

Photocatalysis is considered a promising solution in dealing with serious energy and environmental problems.<sup>6,127</sup> Different from thermal catalysis requires enough heat to cross the energy barrier, photocatalysis

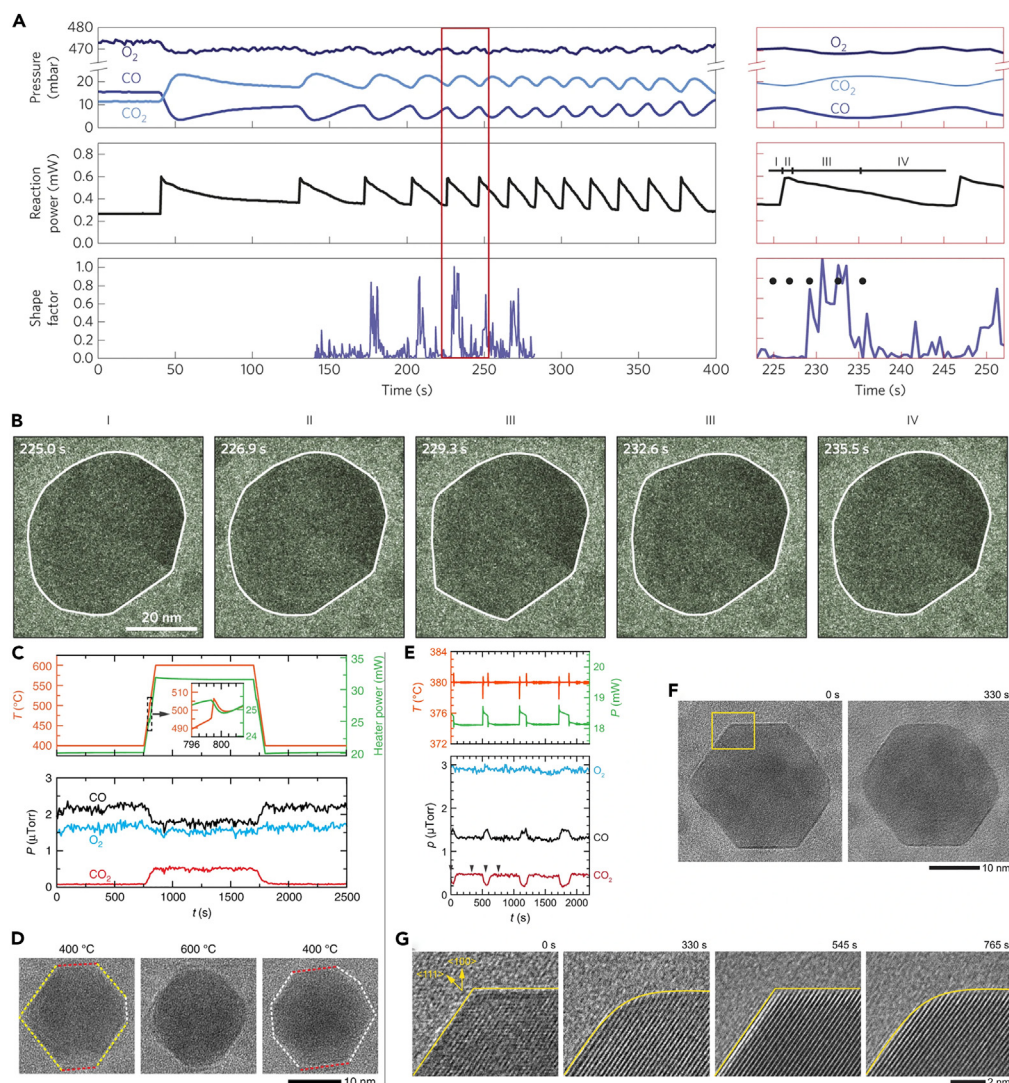


**Figure 9. Structural transformations of catalysts and changes in gas composition during CO oxidation reaction**

(A) The time-dependent mass spectrometry analysis of CO, O<sub>2</sub> and CO<sub>2</sub> pressures, heater power and shape factor for Pt nanoparticles during the CO oxidation reaction.

(B) TEM images series of a Pt nanoparticle during the oscillation. Adapted with permission.<sup>109</sup> Copyright 2014, Nature Publishing Group.

(C) Plots of the measured temperature, heater power, and the corresponding amounts of the CO, O<sub>2</sub>, and CO<sub>2</sub> gases during the CO oxidation reaction in Pt nanoparticles.

(D) TEM images series of a Pd nanoparticle during the oscillation. Adapted with permission.<sup>110</sup> Copyright 2020, Nature Publishing Group.

(E) Plots of the measured temperature, heater power, and the corresponding amounts of the CO, O<sub>2</sub>, and CO<sub>2</sub> gases during the CO oxidation reaction in Pd octahedrons.

(F) TEM image series of a Pd octahedron in low and high-activity states during the oscillation.

(G) HRTEM image series of the Pd octahedron's corner. Adapted with permission.<sup>111</sup> Copyright 2022, Nature Publishing Group.

takes advantage of photogenerated carriers to catalyze the reaction. The photogenerated electrons and holes induced by incident photons need to migrate to the surface of the catalyst for a redox reaction, but suffer continuous recombination in the bulk and surface. The catalyst in the photoexcited state is unusual and inaccessible, and the participation of photogenerated carriers makes the photocatalysis mechanism elusive.<sup>128</sup> Therefore, achieving direct observation of photocatalysts in a photoexcited state and *in*

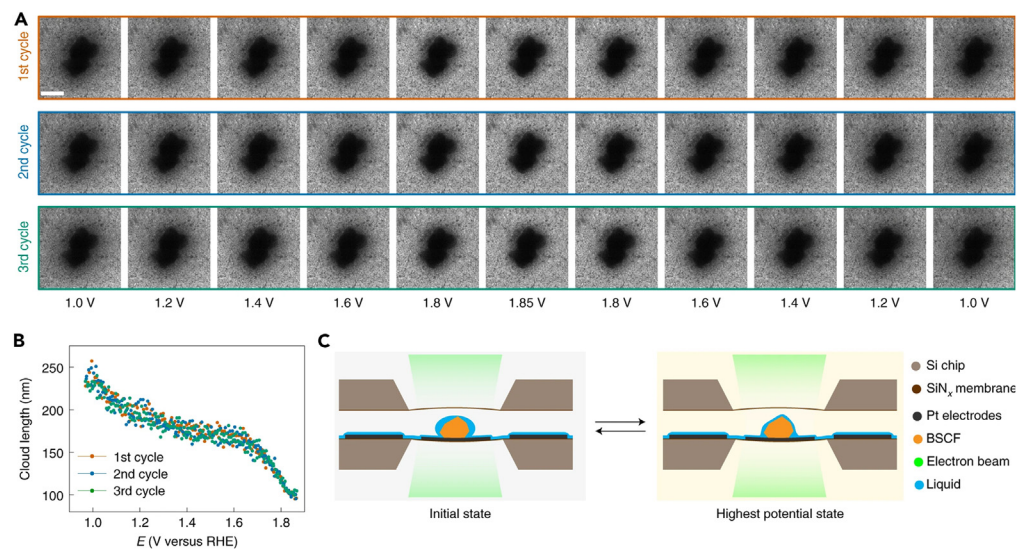


**Figure 10. The wetting behavior of cobalt-based oxide catalysts influenced by an external potential**

(A) Bright-field TEM images at different potential stages during three cycles, ranging from 1.0 to 1.85 V versus RHE.

(B) The length of the cloud surrounding the particles observed in each frame of the TEM images as a function of the applied potential (versus RHE).

(C) Schematic of reversible liquid movement in a liquid cell. Adapted with permission.<sup>122</sup> Copyright 2022, Nature Publishing Group.

*situ* track of the photocatalytic reaction process is of great importance for us to understand the photocatalysis mechanism.

Two different approaches have been proposed for introducing light into TEM, one through a sample holder<sup>129</sup> and the other through an existing port in the microscope column.<sup>130–132</sup> The designed sample holders with optical fiber are well-compatible with the conventional TEM. Light introducing through an existing port is limited to specific TEMs, but can be used in combination with other specialized TEM holders, such as liquid holders.<sup>133</sup>

Molecular adsorption of reactants usually induces surface structure changes of catalysts, which has been confirmed in thermocatalytic reactions, but the light effect on this process is not clear. Zhang and Crozier et al.<sup>51</sup> studied the surface structure evolution of anatase TiO<sub>2</sub> when exposed to light and water vapor by a modified ETEM, in which light was introduced by light fibers (Figure 12). The primary smooth surface became disordered in water vapor under light irradiation, and this disorder only spreads to one or two atom layers on the surface. EELS results suggest that there are Ti<sup>3+</sup> species in the amorphous layer, meaning that some of Ti<sup>4+</sup> have been reduced. The amorphous layer may be related to the surface activation process of TiO<sub>2</sub>, and may generally exist in photocatalytic water splitting processes and provide important reactive sites.

However, the behavior of the photocatalyst under water vapor may not be close to the real state in the actual liquid solution. To approach a realistic photocatalytic reaction, a liquid flow holder was reported, which allows aqueous suspension flow through TEM (Figure 13).<sup>113</sup> It is observed that a surface shell appeared on TiO<sub>2</sub> nanoparticles that were immersed in water and exposed to ultraviolet light. And the thickness of the shell is increasing until hydrogen bubbles generate. EELS and calculation results confirmed the existence of Ti<sup>3+</sup> ions in the surface shell, which may be resulted from the diffusion of hydrogen atoms generated at the H<sub>2</sub>O/TiO<sub>2</sub> interface. In addition, the reconstructed shell on the surface reduced the activation energy of H<sub>2</sub> evolution and facilitated photocatalytic water splitting.

## Challenges for *in situ* TEM in heterogeneous catalysis

### Effects of the electron beam irradiation

As an indispensable light source for TEM imaging, with high energy, the electron beams inevitably interact with the catalysts,<sup>134</sup> aqueous solution<sup>77</sup> and even the windows materials.<sup>135</sup> To reveal the real behavior of

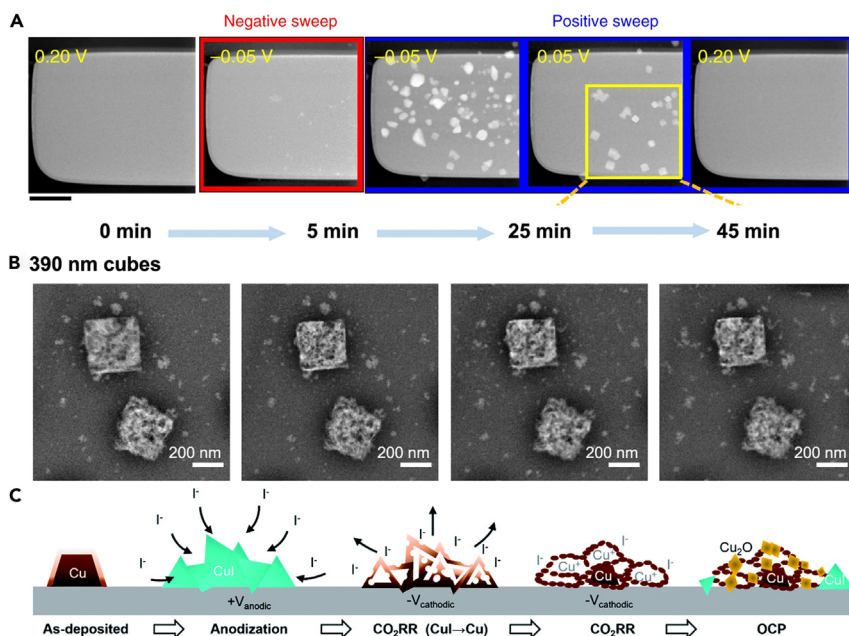


**Figure 11. Electrochemical synthesis and transformation of cubic copper catalysts during CO<sub>2</sub> reduction reaction**

(A) Electrochemical deposition and evolution of copper oxide nanoparticles with voltage variation. Adapted with permission.<sup>124</sup> Copyright 2020, Nature Publishing Group.

(B) Structure evolution of Cu<sub>2</sub>O cubes and small Cu nanoparticles during CO<sub>2</sub> reduction reaction. Adapted with permission.<sup>125</sup> Copyright 2020, Nature Publishing Group.

(C) Schematic illustrating the evolution of iodine-pretreated Cu islands during I-anodization and CO<sub>2</sub> reduction reactions. Adapted with permission.<sup>126</sup> Copyright 2022, The Royal Society of Chemistry.

the catalyst under the reaction conditions, the effect of electron irradiation needs to be studied systematically and eliminated reasonably.

The electron beam with high brightness and high stability is the guarantee of high resolution, but it will also cause irreversible damage to the sample, such as knock-on defects, radiolysis, and electron-stimulated desorption.<sup>15,136</sup> Especially for the metal-organic frameworks (MOFs) and covalent organic frameworks (COFs) which are sensitive to the electron beam, the attack of the electron beam is devastating, which leads to the collapse of the pore structure. Therefore, low-dose imaging technology has been developed, and the specific solutions include a direct-detection electron-counting camera (DDEC) and integrated differential phase contrast scanning transmission electron microscopy (iDPC-STEM). iDPC-STEM can realize the simultaneous imaging of light and heavy element atoms in materials, and greatly improve the imaging quality of electron beam sensitive materials. Taking advantage of iDPC-STEM, Shen and Wei et al.<sup>137</sup> achieved atomic-level imaging of small organic molecules (pyridine and thiophene) in the channel of ZSM-5 sieves at room temperature, and made a breakthrough in single-molecule atomic-level microscopic imaging. Cryo-electron microscopy (cryo-EM) is also a promising method for reducing electron beam damage, and is not only applicable to COF materials,<sup>138</sup> but also valuable for structural analyses of aqueous biological specimens.<sup>139,140</sup> Cryo-EM has demonstrated immense potential in the field of structural biology by utilizing sample freezing, low-dose electron tomography, and three-dimensional reconstruction techniques, leading to the successful visualization of the electron microfacies of macromolecular biological samples.<sup>141</sup> With technological advancements in hardware instruments and analytical software, the resolution of cryo-EM images has significantly improved, showing fascinating prospects in more fields. Notably, Li et al.<sup>142</sup> reported the use of cryo-EM for observing lithium anode materials and performing fine studies of the interface, which marks the rise of cryo-EM in materials science research.

What is more, the electron beam can also interact with the catalysts and reactants in the chemical environment, or even stimulate some reactions. The effect of electron irradiation on Au/TiO<sub>2</sub> in different environments has been studied systematically.<sup>143</sup> It is found that the perimeter interface between the Au

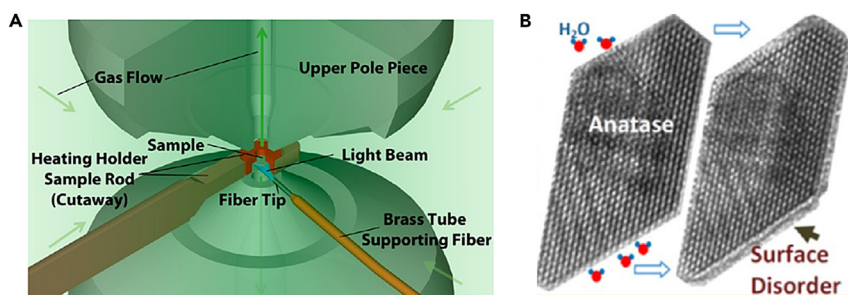


**Figure 12. Structure evolution of TiO<sub>2</sub> nanoparticles under light illumination in water vapor**

(A) Schematic diagram of *in situ* TEM fitted with light fibers.

(B) HRTEM images of TiO<sub>2</sub> nanoparticles before and after UV light illumination in water vapor. Adapted with permission.<sup>51</sup> Copyright 2013, American Chemical Society.

nanoparticles and the TiO<sub>2</sub> support was gradually decorated with Ti species with increasing electron irradiation time. In different chemical environments, Au nanoparticles can even be lifted (in vacuum) or coated (in O<sub>2</sub> atmosphere) with substrates. Similar results had been reported in previous studies of Au/TiO<sub>2</sub><sup>144</sup> and the associated Au/MgO<sup>145</sup> system. Therefore, it is necessary to consider the effect of electron beam during chemical reactions in TEM.

It is worth mentioning that, in the process of nucleation and growth of metal crystals, the electron beam serves as an excitation source, inducing the reduction of the metal from the precursor solution.<sup>115–117</sup> Moreover, the nucleation and growth rate of metal crystals can be controlled by regulating the dose of the electron beam.

In light-induced catalytic reactions, the role of the electron beam needs to be carefully considered. The effect of the electron beam on photocatalytic reactions is more complicated, which interacts with catalysts, aqueous solutions and sacrificial reagents. The high dose of electrons irradiating an aqueous solution will cause radiolysis of liquid, producing hydrogen, oxygen, hydrated proton and hydrated electrons.<sup>146</sup> Ross et al.<sup>147</sup> imaged bubbles nucleation, growth, and migration under electron beam irradiation. The radiolytic species have complex effects, for example, hydrogen ions can change the solution pH,<sup>146</sup> hydrated electrons can react with catalytic reaction media, such as electron sacrifice reagents.<sup>148,149</sup> The phenomenon of beam-induced growth of metallic nanoparticles in aqueous salt solutions via the reduction of metallic cations by highly reactive hydrated electrons is an intriguing avenue for potential beam writing applications.<sup>147,150</sup> What is more, it is important to distinguish between the role of electrons and photons. The intensity of the incident electron beam vastly surpasses that of the illuminating light; therefore, careful selection of effective wavelengths and intensities of light, combined with recording images at a relatively low electron dose rate, is crucial for emphasizing the effect of light illumination and minimizing the influence of the electron beam. However, low exposures result in low signal-to-noise ratio images, necessitating the design of appropriate comparison experiments to eliminate electron beam effects or the timely suspension of the electron beam during light illumination without image recording. Moreover, the integration of direct electron cameras further reduces the electron dose, thus allowing for additional mitigation of electron beam-induced changes during experiments.

### Temporal resolution

High temporal resolution and spatial resolution are two important guarantees for dynamic observation. The enhancement of temporal resolution, facilitated by a variety of methods ranging from video formats to direct-detection cameras capable of generating millisecond frame times, enables the acquisition of more intricate dynamic information regarding the reaction process. The *in situ* imaging of heterogeneous nucleation of individual gold nanocrystals by Jeon et al. with millisecond temporal resolution revealed that the initial phase of atomic crystallization occurs via dynamic structural fluctuations between disordered and crystalline states.<sup>151</sup>

In addition, the implantation of femtosecond laser technology into TEM makes it possible to unravel the nonequilibrium electronic and structural dynamics of a complex transformation.<sup>152,153</sup> Ultrafast TEM (UTEM) permits the imaging of the motion in ultrashort time scales beyond ordinary *in situ* TEM. By utilizing UTEM, the rotational dynamics of Au nanoparticles in an aqueous solution were examined, and a complete

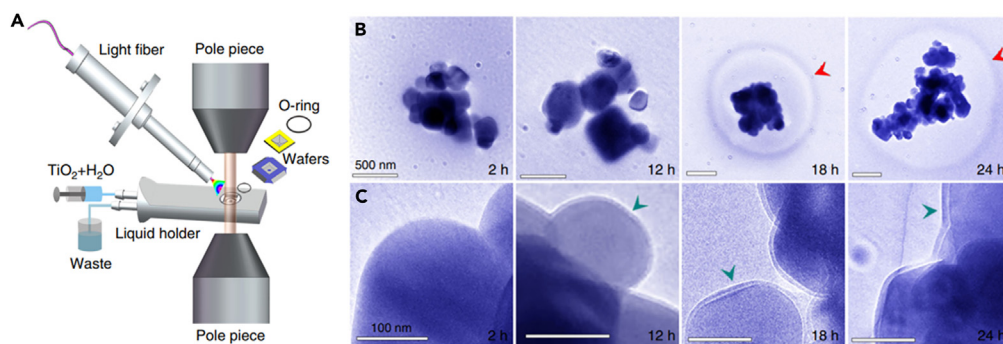


**Figure 13. Structure evolution of TiO<sub>2</sub> nanoparticles under light illumination in liquid solution**

(A) Schematic diagram of *in situ* TEM fitted with a fluidic TEM holder and light fibers.

(B) TEM images of TiO<sub>2</sub> nanoparticles and bubbles formation process.

(C) Enlarged views of the TEM images in (B), showing the growth of the surface shell. Adapted with permission.<sup>113</sup>

Copyright 2018, Nature Publishing Group.

transition from conventional diffusive rotation to the superdiffusive rotation was observed.<sup>154</sup> With the integration of other techniques, TEM has the potential to achieve full time-domain imaging, high spatial resolution, diffraction, and energy spectrum functions.

## Conclusions and outlooks

*In situ* TEM is a versatile and powerful technique that enables direct observation of the dynamic behavior of heterogeneous catalysts across multiple spatial and temporal scales. The application of *in situ* TEM has been extensively employed in the field of heterogeneous catalysis for gas/liquid-solid reactions, yielding a plethora of significant findings encompassing thermal catalysis, electrocatalysis, photocatalysis and beyond (Scheme 1). In gas-solid reactions, the surface reconstruction and shape evolution induced by changes in chemical environments can be observed. Furthermore, the adsorption of gas molecules onto specific sites with regular arrangements on the surface of catalysts may also be witnessed. The integration of TEM, mass spectrometry, and calorimetry enables online analysis of gas products, facilitating the investigation of the intrinsic relationship between structure and activity during reactions. The application of an external voltage to the liquid cell offers a precise approach for correlating the applied electrochemical potential with the microstructural response of the electrocatalysts, facilitating the elucidation of activation and deactivation mechanisms. This strategy represents a fundamental step toward the design of highly stable and efficient electrocatalysts. In addition, *in situ* TEM combined with cryo-electron microscopy also shows great promise in the field of DNA catalysis and enzyme catalysis.

With the successful introduction of the light source, *in situ* TEM has shown great potential in the field of photocatalysis, which was used to investigate the real behavior of photocatalysts under photoexcitation conditions. However, the application of the *in situ* TEM technique in photocatalysis is just emerging in recent years. It is urgent to use such unique and advanced technology for investigating the photocatalytic process and understanding the intrinsic photocatalytic mechanism.

## ACKNOWLEDGMENTS

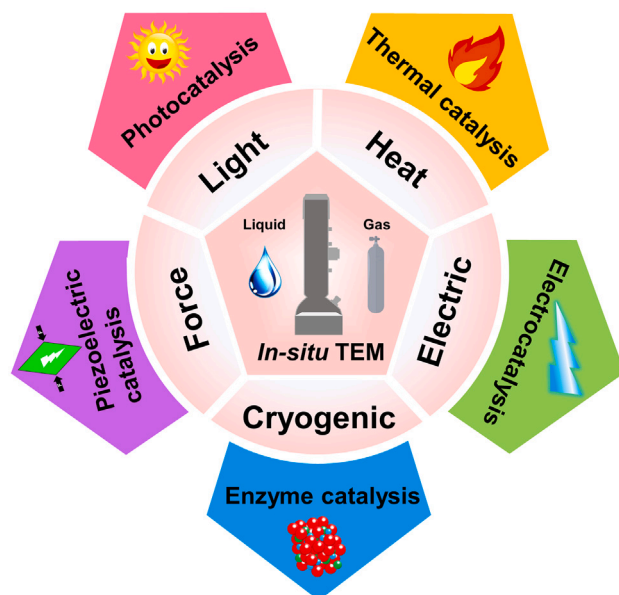
The work was supported by National Natural Science Foundation of China (22090033; 22272165), R.L. would also like to thank the support from Youth Innovation Promotion Association of Chinese Academy of Sciences and the National Youth Talent Support Program.

## AUTHOR CONTRIBUTIONS

R.L. proposed the manuscript framework and outline, J.Q. prepared the manuscript draft, M.S. and R.L. together revised the manuscript.

## DECLARATION OF INTERESTS

The authors declare no competing interest.



**Scheme 1.** *In-situ* TEM and their application in heterogeneous catalysis

## REFERENCES

- Schlögl, R. (2003). Catalytic synthesis of ammonia—a “never-ending story”. *Angew. Chem. Int. Ed.* *42*, 2004–2008. <https://doi.org/10.1002/anie.200301553>.
- Low, J., Yu, J., Jaroniec, M., Wageh, S., and Al-Ghamdi, A.A. (2017). Heterojunction photocatalysts. *Adv. Mater.* *29*, 1601694. <https://doi.org/10.1002/adma.201601694>.
- Seh, Z.W., Kibsgaard, J., Dickens, C.F., Chorkendorff, I., Nørskov, J.K., and Jaramillo, T.F. (2017). Combining theory and experiment in electrocatalysis: insights into materials design. *Science* *355*, eaad4998. <https://doi.org/10.1126/science.aad4998>.
- Zhang, L., Zhao, Z.-J., and Gong, J. (2017). Nanostructured materials for heterogeneous electrocatalytic CO<sub>2</sub> reduction and their related reaction mechanisms. *Angew. Chem. Int. Ed.* *56*, 11326–11353. <https://doi.org/10.1002/anie.201612214>.
- Liu, L., and Corma, A. (2018). Metal catalysts for heterogeneous catalysis: from single atoms to nanoclusters and nanoparticles. *Chem. Rev.* *118*, 4981–5079. <https://doi.org/10.1021/acs.chemrev.7b00776>.
- Hoffmann, M.R., Martin, S.T., Choi, W., and Bahnemann, D.W. (1995). Environmental applications of semiconductor photocatalysis. *Chem. Rev.* *95*, 69–96. <https://doi.org/10.1021/cr00033a004>.
- Gao, W., Hood, Z.D., and Chi, M. (2017). Interfaces in heterogeneous catalysis: advancing mechanistic understanding through atomic-scale measurements. *Acc. Chem. Res.* *50*, 787–795. <https://doi.org/10.1021/acs.accounts.6b00596>.
- Yang, X.-F., Wang, A., Qiao, B., Li, J., Liu, J., and Zhang, T. (2013). Single-atom catalysts: a new frontier in heterogeneous catalysis. *Acc. Chem. Res.* *46*, 1740–1748. <https://doi.org/10.1021/ar300361m>.
- Somorjai, G.A. (1996). Modern surface science and surface technologies: an introduction. *Chem. Rev.* *96*, 1223–1236. <https://doi.org/10.1021/cr950234e>.
- Dou, J., Sun, Z., Opalade, A.A., Wang, N., Fu, W., and Tao, F.F. (2017). Operando Chemistry of catalyst surfaces during catalysis. *Chem. Soc. Rev.* *46*, 2001–2027. <https://doi.org/10.1039/C6CS00931J>.
- Tao, F.F., and Crozier, P.A. (2016). Atomic-scale observations of catalyst structures under reaction conditions and during catalysis. *Chem. Rev.* *116*, 3487–3539. <https://doi.org/10.1021/cr5002657>.
- Tagliavacca, V., Leoni, M., and Weidenthaler, C. (2014). Crystal structure and microstructural changes of molybdenum nitrides traced during catalytic reaction by in situ X-ray diffraction studies. *Phys. Chem. Chem. Phys.* *16*, 6182–6188. <https://doi.org/10.1039/C3CP54578D>.
- Zhang, S., Nguyen, L., Zhu, Y., Zhan, S., Tsung, C.K.F., and Tao, F.F. (2013). In-situ studies of nanocatalysis. *Acc. Chem. Res.* *46*, 1731–1739. <https://doi.org/10.1021/ar300245g>.
- Knoll, M., and Ruska, E. (1932). Das elektronenmikroskop. *Z. Phys.* *78*, 318–339. <https://doi.org/10.1007/BF01342199>.
- Egerton, R.F., Li, P., and Malac, M. (2004). Radiation damage in the tem and sem. *Micron* *35*, 399–409. <https://doi.org/10.1016/j.micron.2004.02.003>.
- Cazaux, J. (1995). Correlations between ionization radiation damage and charging effects in transmission electron microscopy. *Ultramicroscopy* *60*, 411–425. [https://doi.org/10.1016/0304-3991\(95\)00077-1](https://doi.org/10.1016/0304-3991(95)00077-1).
- Dahmen, U., Erni, R., Radmilovic, V., Ksielowski, C., Rossell, M.D., and Denes, P. (2009). Background, status and future of the transmission electron aberration-corrected microscope project. *Philos. Trans. A Math. Phys. Eng. Sci.* *367*, 3795–3808. <https://doi.org/10.1098/rsta.2009.0094>.
- Haider, M., Uhlemann, S., Schwan, E., Rose, H., Kabius, B., and Urban, K. (1998). Electron microscopy image enhanced. *Nature* *392*, 768–769. <https://doi.org/10.1038/33823>.
- Qu, J., Wang, Y., Mu, X., Hu, J., Zeng, B., Lu, Y., Sui, M., Li, R., and Li, C. (2022). Determination of crystallographic orientation and exposed facets of titanium oxide nanocrystals. *Adv. Mater.* *34*, 2203320. <https://doi.org/10.1002/adma.202203320>.
- Qu, J., He, J., Li, H., Jiang, Q., Li, M., Kong, Q., Shi, M., Li, R., and Li, C. (2023). Unraveling the role of interface in photogenerated charge separation at the anatase/rutile heterophase junction. *J. Phys. Chem. C* *127*, 768–775. <https://doi.org/10.1021/acs.jpcc.2c07482>.
- Sun, X., Wu, D., Zou, L., House, S.D., Chen, X., Li, M., Zakharov, D.N., Yang, J.C., and Zhou, G. (2022). Dislocation-induced stop-and-go kinetics of interfacial transformations. *Nature* *607*, 708–713.

- <https://doi.org/10.1038/s41586-022-04880-1>.
22. Song, M., Zhou, G., Lu, N., Lee, J., Nakouzi, E., Wang, H., and Li, D. (2020). Oriented attachment induces fivefold twins by forming and decomposing high-energy grain boundaries. *Science* 367, 40–45. <https://doi.org/10.1126/science.aax6511>.
  23. Ardenne, M.V. (1996). Reminiscences on the origins of the scanning electron microscope and the electron microprobe. In *Advances in Imaging and Electron Physics*, 96, T. Mulvey, ed. (Elsevier), pp. 635–652.
  24. Williams, D.B., and Carter, C.B. (2009). The instrument. In *Transmission Electron Microscopy: A Textbook for Materials Science*, D.B. Williams and C.B. Carter, eds. (Springer US), pp. 141–171.
  25. Browning, N.D., Chisholm, M.F., and Pennycook, S.J. (1993). Atomic-resolution chemical analysis using a scanning transmission electron microscope. *Nature* 366, 143–146. <https://doi.org/10.1038/366143a0>.
  26. Zaluzec, N.J., Burke, M.G., Haigh, S.J., and Kulzick, M.A. (2014). X-ray energy-dispersive spectrometry during in situ liquid cell studies using an analytical electron microscope. *Microsc. Microanal.* 20, 323–329. <https://doi.org/10.1017/S1431927614000154>.
  27. Solmaz, A., Huijben, M., Koster, G., Egoavil, R., Gauquelin, N., Van Tendeloo, G., Verbeeck, J., Noheda, B., and Rijnders, G. (2016). Domain selectivity in Bifeo3 thin films by modified substrate termination. *Adv. Funct. Mater.* 26, 2882–2889. <https://doi.org/10.1002/adfm.201505065>.
  28. Egerton, R.F. (2008). Electron energy-loss spectroscopy in the tem. *Rep. Prog. Phys.* 72, 016502. <https://doi.org/10.1088/0034-4885/72/1/016502>.
  29. Williams, D.B., and Carter, C.B. (2009). Electron energy-loss spectrometers and filters. In *Transmission Electron Microscopy: A Textbook for Materials Science*, D.B. Williams and C.B. Carter, eds. (Springer US), pp. 679–698.
  30. Krivanek, O.L., Dellby, N., Hachtel, J.A., Idrubo, J.C., Hotz, M.T., Plotkin-Swing, B., Bacon, N.J., Bleloch, A.L., Corbin, G.J., Hoffman, M.V., et al. (2019). Progress in ultrahigh energy resolution eels. *Ultramicroscopy* 203, 60–67. <https://doi.org/10.1016/j.ultramic.2018.12.006>.
  31. Longo, P., Thomas, P.J., and Twesten, R.D. (2012). Atomic-level eels mapping using high-energy edges in Dualeels™ mode. *Microsc. Today* 20, 30–36. <https://doi.org/10.1017/s1551929512000478>.
  32. Longo, P., Thomas, P.J., Aitouchen, A., Rice, P., Topuria, T., and Twesten, R.D. (2015). Atomic elemental and chemical analysis of strtio3/lamno3 multilayers using fast simultaneous eels and eds analysis in digitalmicrograph. *Microsc. Today* 23, 44–53. <https://doi.org/10.1017/s1551929515000589>.
  33. Suenaga, K., and Koshino, M. (2010). Atom-by-Atom spectroscopy at graphene edge. *Nature* 468, 1088–1090. <https://doi.org/10.1038/nature09664>.
  34. Tanaka, N., Usukura, J., Kusunoki, M., Saito, Y., Sasaki, K., Tanji, T., Muto, S., and Arai, S. (2013). Development of an environmental high-voltage electron microscope for reaction science. *Microscopy (Oxf)* 62, 205–215. <https://doi.org/10.1093/jmicro/dfs095>.
  35. Wagner, J.B., Cavalca, F., Damsgaard, C.D., Duchstein, L.D.L., and Hansen, T.W. (2012). Exploring the environmental transmission electron microscope. *Micron* 43, 1169–1175. <https://doi.org/10.1016/j.micron.2012.02.008>.
  36. Hansen, T.W., and Wagner, J.B. (2012). Environmental transmission electron microscopy in an aberration-corrected environment. *Microsc. Microanal.* 18, 684–690. <https://doi.org/10.1017/S1431927612000293>.
  37. Boyes, E.D., and Gai, P.L. (1997). Environmental high resolution electron microscopy and applications to chemical science. *Ultramicroscopy* 67, 219–232. [https://doi.org/10.1016/S0304-3991\(96\)00099-X](https://doi.org/10.1016/S0304-3991(96)00099-X).
  38. Wu, J., Shan, H., Chen, W., Gu, X., Tao, P., Song, C., Shang, W., and Deng, T. (2016). In situ environmental tem in imaging gas and liquid phase chemical reactions for materials research. *Adv. Mater.* 28, 9686–9712. <https://doi.org/10.1002/adma.201602519>.
  39. Jinschek, J.R., and Helveg, S. (2012). Image resolution and sensitivity in an environmental transmission electron microscope. *Micron* 43, 1156–1168. <https://doi.org/10.1016/j.micron.2012.01.006>.
  40. Ashraf, M.W., Tayyaba, S., and Afzulpurkar, N. (2011). Micro electromechanical systems (mems) based microfluidic devices for biomedical applications. *Int. J. Mol. Sci.* 12, 3648–3704. <https://doi.org/10.3390/ijms12063648>.
  41. Ho, C.-M., and Tai, Y.-C. (1998). Micro-electro-mechanical-systems (mems) and fluid flows. *Annu. Rev. Fluid Mech.* 30, 579–612. <https://doi.org/10.1146/annurev.fluid.30.1.579>.
  42. Hansen, T.W., and Wagner, J.B. (2014). Catalysts under controlled atmospheres in the transmission electron microscope. *ACS Catal.* 4, 1673–1685. <https://doi.org/10.1021/cs401148d>.
  43. Liao, H.-G., and Zheng, H. (2016). Liquid cell transmission electron microscopy. *Annu. Rev. Phys. Chem.* 67, 719–747. <https://doi.org/10.1146/annurev-physchem-040215-112501>.
  44. Wu, F., and Yao, N. (2015). Advances in windowed gas cells for in-situ tem studies. *Nano Energy* 13, 735–756. <https://doi.org/10.1016/j.nanoen.2015.03.015>.
  45. Duan, M., Yu, J., Meng, J., Zhu, B., Wang, Y., and Gao, Y. (2018). Reconstruction of supported metal nanoparticles in reaction conditions. *Angew Chem. Int. Ed. Engl.* 57, 6464–6469. <https://doi.org/10.1002/anie.201800925>.
  46. Helveg, S., López-Cartes, C., Sehested, J., Hansen, P.L., Clausen, B.S., Rostrup-Nielsen, J.R., Abild-Pedersen, F., and Nørskov, J.K. (2004). Atomic-scale imaging of carbon nanofibre growth. *Nature* 427, 426–429. <https://doi.org/10.1038/nature02278>.
  47. Kuo, C.H., Yang, Y.C., Gwo, S., and Huang, M.H. (2011). Facet-dependent and Au nanocrystal-enhanced electrical and photocatalytic properties of Au-Cu2o core-shell heterostructures. *J. Am. Chem. Soc.* 133, 1052–1057. <https://doi.org/10.1021/ja109182y>.
  48. Zhang, L., Yang, T., Du, C., Liu, Q., Tang, Y., Zhao, J., Wang, B., Chen, T., Sun, Y., Jia, P., et al. (2020). Lithium whisker growth and stress generation in an in situ atomic force microscope-environmental transmission electron microscope set-up. *Nat. Nanotechnol.* 15, 94–98. <https://doi.org/10.1038/s41565-019-0604-x>.
  49. Gao, P., Kang, Z., Fu, W., Wang, W., Bai, X., and Wang, E. (2010). Electrically driven redox process in cerium oxides. *J. Am. Chem. Soc.* 132, 4197–4201. <https://doi.org/10.1021/ja9086616>.
  50. Chen, P., Zhong, X., Zorn, J.A., Li, M., Sun, Y., Abid, A.Y., Ren, C., Li, Y., Li, X., Ma, X., et al. (2020). Atomic imaging of mechanically induced topological transition of ferroelectric vortices. *Nat. Commun.* 11, 1840. <https://doi.org/10.1038/s41467-020-15616-y>.
  51. Zhang, L., Miller, B.K., and Crozier, P.A. (2013). Atomic level in situ observation of surface amorphization in anatase nanocrystals during light irradiation in water vapor. *Nano Lett.* 13, 679–684. <https://doi.org/10.1021/nl304333h>.
  52. Ring, E.A., and de Jonge, N. (2010). Microfluidic system for transmission electron microscopy. *Microsc. Microanal.* 16, 622–629. <https://doi.org/10.1017/S1431927610093669>.
  53. de Jonge, N., and Ross, F.M. (2011). Electron microscopy of specimens in liquid. *Nat. Nanotechnol.* 6, 695–704. <https://doi.org/10.1038/nnano.2011.161>.
  54. Ruska, E. (1942). Beitrag zur übermikroskopischen abbildung bei höheren drucken. *Kolloid Z.* 100, 212–219. <https://doi.org/10.1007/BF01519549>.
  55. Hashimoto, H., Naiki, T., Eto, T., and Fujiwara, K. (1968). High temperature gas reaction specimen chamber for an electron microscope. *Jpn. J. Appl. Phys.* 7, 946–952. <https://doi.org/10.1143/jjap.7.946>.
  56. Kamino, T., Yaguchi, T., Konno, M., Watabe, A., Marukawa, T., Mima, T., Kuroda, K., Saka, H., Arai, S., Makino, H., et al. (2005). Development of a gas injection/specimen heating holder for use with transmission electron microscope. *J. Electron. Microsc.* 54, 497–503. <https://doi.org/10.1093/jmicro/dfi071>.

57. Yuan, W., Zhu, B., Li, X.Y., Hansen, T.W., Ou, Y., Fang, K., Yang, H., Zhang, Z., Wagner, J.B., Gao, Y., and Wang, Y. (2020). Visualizing H<sub>2</sub>O molecules reacting at TiO<sub>2</sub> active sites with transmission electron microscopy. *Science* 367, 428–430. <https://doi.org/10.1126/science.aay2474>.
58. Heide, H.G. (1962). Electron microscopic observation of specimens under controlled gas pressure. *J. Cell Biol.* 13, 147–152. <https://doi.org/10.1083/jcb.13.1.147>.
59. Parkinson, G.M. (1989). High resolution, in-situ controlled atmosphere transmission electron microscopy (catem) of heterogeneous catalysts. *Catal. Lett.* 2, 303–307. <https://doi.org/10.1007/BF00770228>.
60. Daulton, T.L., Little, B.J., Lowe, K., and Jones-Meehan, J. (2001). In situ environmental cell-transmission electron microscopy study of microbial reduction of chromium(vi) using electron energy loss spectroscopy. *Microsc. Microanal.* 7, 470–485. <https://doi.org/10.1007/S10005-001-0021-3>.
61. Creemer, J.F., Helveg, S., Hoveling, G.H., Ullmann, S., Molenbroek, A.M., Sarro, P.M., and Zandbergen, H.W. (2008). Atomic-scale electron microscopy at ambient pressure. *Ultramicroscopy* 108, 993–998. <https://doi.org/10.1016/j.ultramic.2008.04.014>.
62. Alan, T., Yokosawa, T., Gaspar, J., Pandraud, G., Paul, O., Creemer, F., Sarro, P.M., and Zandbergen, H.W. (2012). Micro-fabricated channel with ultra-thin yet ultra-strong windows enables electron microscopy under 4-bar pressure. *Appl. Phys. Lett.* 100, 081903. <https://doi.org/10.1063/1.3688490>.
63. de Jonge, N., Bigelow, W.C., and Veith, G.M. (2010). Atmospheric pressure scanning transmission electron microscopy. *Nano Lett.* 10, 1028–1031. <https://doi.org/10.1021/nl904254g>.
64. Williamson, M.J., Tromp, R.M., Vereecken, P.M., Hull, R., and Ross, F.M. (2003). Dynamic microscopy of nanoscale cluster growth at the solid-liquid interface. *Nat. Mater.* 2, 532–536. <https://doi.org/10.1038/nmat944>.
65. de Jonge, N., Houben, L., Dunin-Borkowski, R.E., and Ross, F.M. (2018). Resolution and aberration correction in liquid cell transmission electron microscopy. *Nat. Rev. Mater.* 4, 61–78. <https://doi.org/10.1038/s41578-018-0071-2>.
66. Keskin, S., Kunas, P., and de Jonge, N. (2019). Liquid-phase electron microscopy with controllable liquid thickness. *Nano Lett.* 19, 4608–4613. <https://doi.org/10.1021/acs.nanolett.9b01576>.
67. Holtz, M.E., Yu, Y., Gao, J., Abruña, H.D., and Muller, D.A. (2013). In Situ electron energy-loss spectroscopy in liquids. *Microsc. Microanal.* 19, 1027–1035. <https://doi.org/10.1017/S1431927613001505>.
68. Beker, A.F., Sun, H., Lemang, M., van Omme, J.T., Spruit, R.G., Bremmer, M., Basak, S., and Pérez Garza, H.H. (2020). In situ electrochemistry inside a tem with controlled mass transport. *Nanoscale* 12, 22192–22201. <https://doi.org/10.1039/D0NR04961A>.
69. Park, J., Koo, K., Noh, N., Chang, J.H., Cheong, J.Y., Dae, K.S., Park, J.S., Ji, S., Kim, I.-D., and Yuk, J.M. (2021). Graphene liquid cell electron microscopy: progress, applications, and perspectives. *ACS Nano* 15, 288–308. <https://doi.org/10.1021/acsnano.0c10229>.
70. Yuk, J.M., Park, J., Ercius, P., Kim, K., Hellebusch, D.J., Crommie, M.F., Lee, J.Y., Zettl, A., and Alivisatos, A.P. (2012). High-resolution em of colloidal nanocrystal growth using graphene liquid cells. *Science* 336, 61–64. <https://doi.org/10.1126/science.1217654>.
71. Koo, K., Dae, K.S., Hahn, Y.K., and Yuk, J.M. (2020). Live cell electron microscopy using graphene veils. *Nano Lett.* 20, 4708–4713. <https://doi.org/10.1021/acs.nanolett.0c00715>.
72. Cho, H., Jones, M.R., Nguyen, S.C., Hauwiler, M.R., Zettl, A., and Alivisatos, A.P. (2017). The use of graphene and its derivatives for liquid-phase transmission electron microscopy of radiation-sensitive specimens. *Nano Lett.* 17, 414–420. <https://doi.org/10.1021/acs.nanolett.6b04383>.
73. Clark, N., Kelly, D.J., Zhou, M., Zou, Y.-C., Myung, C.W., Hopkinson, D.G., Schran, C., Michaelides, A., Gorbachev, R., and Haigh, S.J. (2022). Tracking single adatoms in liquid in a transmission electron microscope. *Nature* 609, 942–947. <https://doi.org/10.1038/s41586-022-05130-0>.
74. Yoshida, H., Kuwauchi, Y., Jinschek, J.R., Sun, K., Tanaka, S., Kohyama, M., Shimada, S., Haruta, M., and Takeda, S. (2012). Visualizing gas molecules interacting with supported nanoparticulate catalysts at reaction conditions. *Science* 335, 317–319. <https://doi.org/10.1126/science.1213194>.
75. Mehraeen, S., McKeown, J.T., Deshmukh, P.V., Evans, J.E., Abellan, P., Xu, P., Reed, B.W., Taheri, M.L., Fischione, P.E., and Browning, N.D. (2013). A (S)tem gas cell holder with localized laser heating for in situ experiments. *Microsc. Microanal.* 19, 470–478. <https://doi.org/10.1017/s1431927612014419>.
76. Sharma, R. (2001). Design and applications of environmental cell transmission electron microscope for in situ observations of gas-solid reactions. *Microsc. Microanal.* 7, 494–506. <https://doi.org/10.1007/S10005-001-0015-1>.
77. Ross, F.M. (2015). Opportunities and challenges in liquid cell electron microscopy. *Science* 350, aaa9886. <https://doi.org/10.1126/science.aaa9886>.
78. Kelly, D.J., Zhou, M., Clark, N., Hamer, M.J., Lewis, E.A., Rakowski, A.M., Haigh, S.J., and Gorbachev, R.V. (2018). Nanometer resolution elemental mapping in graphene-based tem liquid cells. *Nano Lett.* 18, 1168–1174. <https://doi.org/10.1021/acs.nanolett.7b04713>.
79. Rasool, H., Dunn, G., Fathalizadeh, A., and Zettl, A. (2016). Graphene-sealed Si/sin cavities for high-resolution in situ electron microscopy of nano-confined solutions. *Phys. Status Solidi B* 253, 2351–2354. <https://doi.org/10.1002/pssb.201600232>.
80. Textor, M., and de Jonge, N. (2018). Strategies for preparing graphene liquid cells for transmission electron microscopy. *Nano Lett.* 18, 3313–3321. <https://doi.org/10.1021/acs.nanolett.8b01366>.
81. Thiel, P.A., and Madey, T.E. (1987). The interaction of water with solid surfaces: fundamental aspects. *Surf. Sci. Rep.* 7, 211–385. [https://doi.org/10.1016/0167-5729\(87\)90001-X](https://doi.org/10.1016/0167-5729(87)90001-X).
82. Marković, N.M., and Ross, P.N. (2002). Surface science studies of model fuel cell electrocatalysts. *Surf. Sci. Rep.* 45, 117–229. [https://doi.org/10.1016/S0167-5729\(01\)00022-X](https://doi.org/10.1016/S0167-5729(01)00022-X).
83. Lugg, N.R., Kothleitner, G., Shibata, N., and Ikuhara, Y. (2015). On the quantitiveness of. *Ultramicroscopy* 151, 150–159. <https://doi.org/10.1016/j.ultramic.2014.11.029>.
84. Yin, Z.-W., Zhao, W., Li, J., Peng, X., Lin, C., Zhang, M., Zeng, Z., Liao, H., Chen, H., Lin, H., and Pan, F. (2022). Advanced electron energy loss spectroscopy for battery studies. *Adv. Funct. Mater.* 32, 2107190. <https://doi.org/10.1002/adfm.202107190>.
85. Espinosa-Magaña, F., Rosas, A., Esparza-Ponce, H.E., Ochoa-Lara, M.T., and Aguilar-Elguezabal, A. (2009). In situ study of the metal-insulator transition in vo<sub>2</sub> by eels and ab initio calculations. *Micron* 40, 787–792. <https://doi.org/10.1016/j.micron.2009.07.007>.
86. Uchikawa, H. (2001). Specialized techniques. In *Handbook of Analytical Techniques in Concrete Science and Technology*, V.S. Ramachandran and J.J. Beaudoin, eds. (William Andrew Publishing), pp. 820–934.
87. Smith, R., Inomata, H., and Peters, C. (2013). Chemical equilibria and reaction kinetics. In *Supercritical Fluid Science and Technology*, 4, R. Smith, H. Inomata, and C. Peters, eds. (Elsevier), pp. 617–688.
88. Chanda, S., and Mehendale, H.M. (2005). Acenaphthene. In *Encyclopedia of Toxicology*, Second Edition, P. Wexler, ed. (Elsevier), pp. 11–13.
89. Matsuda, R., Kitaura, R., Kitagawa, S., Kubota, Y., Belosludov, R.V., Kobayashi, T.C., Sakamoto, H., Chiba, T., Takata, M., Kawazoe, Y., and Mita, Y. (2005). Highly controlled acetylene accommodation in a metal-organic microporous. *Nature* 436, 238–241. <https://doi.org/10.1038/nature03852>.
90. Hammer, B., Morikawa, Y., and Nørskov, J.K. (1996). Co chemisorption at metal surfaces and overlayers. *Phys. Rev. Lett.* 76, 2141–2144. <https://doi.org/10.1103/PhysRevLett.76.2141>.
91. Vittadini, A., Selloni, A., Rotzinger, F.P., and Grätzel, M. (1998). Structure and energetics of water adsorbed at TiO<sub>2</sub> anatase (101) and

- (001) surfaces. *Phys. Rev. Lett.* **81**, 2954–2957. <https://doi.org/10.1103/PhysRevLett.81.2954>.
92. Miller, B.K., and Crozier, P.A. (2014). Analysis of catalytic gas products using electron energy-loss spectroscopy and residual gas analysis for operando transmission electron microscopy. *Microsc. Microanal.* **20**, 815–824. <https://doi.org/10.1017/s1431927614000749>.
93. Zhang, X., Han, S., Zhu, B., Zhang, G., Li, X., Gao, Y., Wu, Z., Yang, B., Liu, Y., Baaziz, W., et al. (2020). Reversible loss of core-shell structure for Ni-Au bimetallic nanoparticles during Co<sub>2</sub> hydrogenation. *Nat. Catal.* **3**, 411–417. <https://doi.org/10.1038/s41929-020-0440-2>.
94. Li, Q., Wang, P., Feng, Q., Mao, M., Liu, J., Mao, S.X., and Wang, H. (2014). In situ tem on the reversibility of nanosized Sn anodes during the electrochemical reaction. *Chem. Mater.* **26**, 4102–4108. <https://doi.org/10.1021/cm5009448>.
95. Zhu, K., Zhu, X., and Yang, W. (2019). Application of in situ techniques for the characterization of nife-based oxygen evolution reaction (oer) electrocatalysts. *Angew. Chem. Int. Ed.* **58**, 1252–1265. <https://doi.org/10.1002/anie.201802923>.
96. Hansen, P.L., Wagner, J.B., Helveg, S., Rostrup-Nielsen, J.R., Clausen, B.S., and Topsøe, H. (2002). Atom-resolved imaging of dynamic shape changes in supported copper nanocrystals. *Science* **295**, 2053–2055. <https://doi.org/10.1126/science.1069325>.
97. Jiang, Y., Li, H., Wu, Z., Ye, W., Zhang, H., Wang, Y., Sun, C., and Zhang, Z. (2016). In situ observation of hydrogen-induced surface faceting for palladium-copper nanocrystals at atmospheric pressure. *Angew. Chem. Int. Ed. Engl.* **55**, 12427–12430. <https://doi.org/10.1002/anie.201605956>.
98. Zhang, S., Plessow, P.N., Willis, J.J., Dai, S., Xu, M., Graham, G.W., Cargnello, M., Abild-Pedersen, F., and Pan, X. (2016). Dynamical observation and detailed description of catalysts under strong metal-support interaction. *Nano Lett.* **16**, 4528–4534. <https://doi.org/10.1021/acs.nanolett.6b01769>.
99. Wang, L.-N., Li, X.-N., and He, S.-G. (2020). Recent research progress in the study of catalytic Co oxidation by gas phase atomic clusters. *Sci. China Mater.* **63**, 892–902. <https://doi.org/10.1007/s40843-019-1206-2>.
100. Yuan, W., Zhu, B., Fang, K., Li, X.Y., Hansen, T.W., Ou, Y., Yang, H., Wagner, J.B., Gao, Y., Wang, Y., and Zhang, Z. (2021). In situ manipulation of the active Au-TiO<sub>2</sub> interface with atomic precision during Co oxidation. *Science* **371**, 517–521. <https://doi.org/10.1126/science.abe3558>.
101. Frey, H., Beck, A., Huang, X., van Bokhoven, J.A., and Willinger, M.G. (2022). Dynamic interplay between metal nanoparticles and oxide support under redox conditions. *Science* **376**, 982–987. <https://doi.org/10.1126/science.abm3371>.
102. Jaramillo, T.F., Jørgensen, K.P., Bonde, J., Nielsen, J.H., Hørch, S., and Chorkendorff, I. (2007). Identification of active edge sites for electrochemical H<sub>2</sub> evolution from MoS<sub>2</sub> nanocatalysts. *Science* **317**, 100–102. <https://doi.org/10.1126/science.1141483>.
103. Stamenkovic, V.R., Fowler, B., Mun, B.S., Wang, G., Ross, P.N., Lucas, C.A., and Marković, N.M. (2007). Improved oxygen reduction activity on Pt<sub>3</sub>Ni(111) via increased surface site availability. *Science* **315**, 493–497. <https://doi.org/10.1126/science.1135941>.
104. Kalz, K.F., Kraehnert, R., Dvoyashkin, M., Dittmeyer, R., Gläser, R., Krewer, U., Reuter, K., and Grunwaldt, J.-D. (2017). Future challenges in heterogeneous catalysis: understanding catalysts under dynamic reaction conditions. *ChemCatChem* **9**, 17–29. <https://doi.org/10.1002/cctc.201600996>.
105. Yuan, W., Wu, H., Li, H., Dai, Z., Zhang, Z., Sun, C., and Wang, Y. (2017). In situ stem determination of the atomic structure and reconstruction mechanism of the TiO<sub>2</sub> (001) (1 × 4) surface. *Chem. Mater.* **29**, 3189–3194. <https://doi.org/10.1021/acs.chemmater.7b00284>.
106. Vincent, J.L., and Crozier, P.A. (2021). Atomic level fluxional behavior and activity of ceo<sub>2</sub>-supported Pt catalysts for Co oxidation. *Nat. Commun.* **12**, 5789. <https://doi.org/10.1038/s41467-021-26047-8>.
107. Plodinec, M., Nerl, H.C., Girgsdies, F., Schlögl, R., and Lunkenbein, T. (2020). Insights into chemical dynamics and their impact on the reactivity of Pt nanoparticles during Co oxidation by operando tem. *ACS Catal.* **10**, 3183–3193. <https://doi.org/10.1021/acscatal.9b03692>.
108. Miller, B.K., and Crozier, P.A. (2021). Linking changes in reaction kinetics and atomic-level surface structures on a supported Ru catalyst for Co oxidation. *ACS Catal.* **11**, 1456–1463. <https://doi.org/10.1021/acscatal.0c03789>.
109. Vendelbo, S.B., Elkjær, C.F., Falsig, H., Puspitasari, I., Dona, P., Mele, L., Morana, B., Nelissen, B.J., van Rijn, R., Creemer, J.F., et al. (2014). Visualization of oscillatory behaviour of Pt nanoparticles catalysing Co oxidation. *Nat. Mater.* **13**, 884–890. <https://doi.org/10.1038/nmat4033>.
110. Chee, S.W., Arce-Ramos, J.M., Li, W., Genest, A., and Mirsaidov, U. (2020). Structural changes in noble metal nanoparticles during Co oxidation and their impact on catalyst activity. *Nat. Commun.* **11**, 2133. <https://doi.org/10.1038/s41467-020-16027-9>.
111. Ghosh, T., Arce-Ramos, J.M., Li, W.-Q., Yan, H., Chee, S.W., Genest, A., and Mirsaidov, U. (2022). Periodic structural changes in Pd nanoparticles during oscillatory Co oxidation reaction. *Nat. Commun.* **13**, 6176. <https://doi.org/10.1038/s41467-022-33304-x>.
112. Ortiz Peña, N., Ihiawakrim, D., Han, M., Lassalle-Kaiser, B., Carencro, S., Sanchez, C., Laberty-Robert, C., Portehault, D., and Ersen, O. (2019). Morphological and structural evolution of Co<sub>3</sub>O<sub>4</sub> nanoparticles revealed by in situ electrochemical transmission electron microscopy during electrocatalytic water oxidation. *ACS Nano* **13**, 11372–11381. <https://doi.org/10.1021/acsnano.9b04745>.
113. Lu, Y., Yin, W.J., Peng, K.L., Wang, K., Hu, Q., Selloni, A., Chen, F.R., Liu, L.M., and Sui, M.L. (2018). Self-hydrogenated shell promoting photocatalytic H<sub>2</sub> evolution on anatase TiO<sub>2</sub>. *Nat. Commun.* **9**, 2752. <https://doi.org/10.1038/s41467-018-05144-1>.
114. Hong, J., Bae, J.H., Jo, H., Park, H.Y., Lee, S., Hong, S.J., Chun, H., Cho, M.K., Kim, J., Kim, J., et al. (2022). Metastable hexagonal close-packed palladium hydride in liquid cell tem. *Nature* **603**, 631–636. <https://doi.org/10.1038/s41586-021-04391-5>.
115. Liao, H.-G., Cui, L., Whitlam, S., and Zheng, H. (2012). Real-time imaging of Pt<sub>3</sub>Fe nanorod growth in solution. *Science* **336**, 1011–1014. <https://doi.org/10.1126/science.1219185>.
116. Zheng, H., Smith, R.K., Jun, Y.-w., Kisielowski, C., Dahmen, U., and Alivisatos, A.P. (2009). Observation of single colloidal platinum nanocrystal growth trajectories. *Science* **324**, 1309–1312. <https://doi.org/10.1126/science.1172104>.
117. Liao, H.-G., Zherebetsky, D., Xin, H., Czarnik, C., Ercius, P., Emlund, H., Pan, M., Wang, L.-W., and Zheng, H. (2014). Facet development during platinum nanocube growth. *Science* **345**, 916–919. <https://doi.org/10.1126/science.1253149>.
118. Impagnatiello, A., Cerqueira, C.F., Coulon, P.-E., Morin, A., Escibano, S., Guetaz, L., Clochard, M.-C., and Rizza, G. (2020). Degradation mechanisms of supported Pt nanocatalysts in proton exchange membrane fuel cells: an operando study through liquid cell transmission electron microscopy. *ACS Appl. Energy Mater.* **3**, 2360–2371. <https://doi.org/10.1021/acsaem.9b02000>.
119. Vavra, J., Shen, T.-H., Stoian, D., Tileli, V., and Buonsanti, R. (2021). Real-time monitoring reveals dissolution/redeposition mechanism in copper nanocatalysts during the initial stages of the Co<sub>2</sub> reduction reaction. *Angew. Chem. Int. Ed.* **60**, 1347–1354. <https://doi.org/10.1002/anie.202011137>.
120. Wang, L., and Xiao, F.S. (2014). The importance of catalyst wettability. *ChemCatChem* **6**, 3048–3052. <https://doi.org/10.1002/cctc.201402437>.
121. Zhang, Q., Li, T., Liang, J., Wang, N., Kong, X., Wang, J., Qian, H., Zhou, Y., Liu, F., Wei, C., et al. (2018). Highly wettable and metallic nife-phosphate/phosphide catalyst synthesized by plasma for highly efficient oxygen evolution reaction. *J. Mater. Chem.* **6**, 7509–7516. <https://doi.org/10.1039/C8TA01334A>.
122. Shen, T.-H., Spillane, L., Peng, J., Shao-Horn, Y., and Tileli, V. (2022). Switchable wetting of oxygen-evolving oxide catalysts.

- Nat. Catal. 5, 30–36. <https://doi.org/10.1038/s41929-021-00723-w>.
123. Beermann, V., Holtz, M.E., Padgett, E., de Araujo, J.F., Muller, D.A., and Strasser, P. (2019). Real-time imaging of activation and degradation of carbon supported octahedral Pt–Ni alloy fuel cell catalysts at the nanoscale using in situ electrochemical liquid cell stem. *Energy Environ. Sci.* 12, 2476–2485. <https://doi.org/10.1039/C9EE01185D>.
  124. Arán-Ais, R.M., Rizo, R., Grosse, P., Algara-Siller, G., Dembélé, K., Plodinec, M., Lunkenbein, T., Chee, S.W., and Cuenya, B.R. (2020). Imaging electrochemically synthesized Cu<sub>2</sub>O cubes and their morphological evolution under conditions relevant to Co<sub>2</sub> electroreduction. *Nat. Commun.* 11, 3489. <https://doi.org/10.1038/s41467-020-17220-6>.
  125. Grosse, P., Yoon, A., Rettenmaier, C., Herzog, A., Chee, S.W., and Roldan Cuenya, B. (2021). Dynamic transformation of cubic copper catalysts during Co<sub>2</sub> electroreduction and its impact on catalytic selectivity. *Nat. Commun.* 12, 6736. <https://doi.org/10.1038/s41467-021-26743-5>.
  126. Yoon, A., Poon, J., Grosse, P., Chee, S.W., and Cuenya, B.R. (2022). Iodide-mediated Cu catalyst restructuring during Co<sub>2</sub> electroreduction. *J. Mater. Chem.* 10, 14041–14050. <https://doi.org/10.1039/D1TA11089F>.
  127. Schneider, J., Matsuoka, M., Takeuchi, M., Zhang, J., Horiuchi, Y., Anpo, M., and Bahnemann, D.W. (2014). Understanding TiO<sub>2</sub> photocatalysis: mechanisms and materials. *Chem. Rev.* 114, 9919–9986. <https://doi.org/10.1021/cr5001892>.
  128. Tao, X., Shi, W., Zeng, B., Zhao, Y., Ta, N., Wang, S., Adenle, A.A., Li, R., and Li, C. (2020). Photoinduced surface activation of semiconductor photocatalysts under reaction conditions: a commonly overlooked phenomenon in photocatalysis. *ACS Catal.* 10, 5941–5948. <https://doi.org/10.1021/acscatal.0c00462>.
  129. Cavalca, F., Laursen, A.B., Kardynal, B.E., Dunin-Borkowski, R.E., Dahl, S., Wagner, J.B., and Hansen, T.W. (2012). In situ transmission electron microscopy of light-induced photocatalytic reactions. *Nanotechnology* 23, 075705. <https://doi.org/10.1088/0957-4484/23/7/075705>.
  130. Miller, B.K., and Crozier, P.A. (2015). Resolving surface structures of catalytic Ru nanoparticles during catalysis. *Microsc. Microanal.* 21, 567–568. <https://doi.org/10.1017/S1431927615003633>.
  131. Yoshida, K., Yamasaki, J., and Tanaka, N. (2004). In situ high-resolution transmission electron microscopy observation of photodecomposition process of polyhydrocarbons on catalytic TiO<sub>2</sub> films. *Appl. Phys. Lett.* 84, 2542–2544. <https://doi.org/10.1063/1.1689747>.
  132. Yoshida, K., Nozaki, T., Hirayama, T., and Tanaka, N. (2007). In situ high-resolution transmission electron microscopy of photocatalytic reactions by excited electrons in ionic liquid. *J. Electron. Microsc.* 56, 177–180. <https://doi.org/10.1093/jmicro/dfm021>.
  133. Kadkhodazadeh, S., Cavalca, F.C., Miller, B.J., Zhang, L., Wagner, J.B., Crozier, P.A., and Hansen, T.W. (2022). In situ tem under optical excitation for catalysis research. *Top. Curr. Chem.* 380, 52. <https://doi.org/10.1007/s41061-022-00408-3>.
  134. Yin, Z.-W., Betzler, S.B., Sheng, T., Zhang, Q., Peng, X., Shanguan, J., Bustillo, K.C., Li, J.-T., Sun, S.-G., and Zheng, H. (2019). Visualization of facet-dependent pseudophotocatalytic behavior of TiO<sub>2</sub> nanorods for water splitting using in situ liquid cell tem. *Nano Energy* 62, 507–512. <https://doi.org/10.1016/j.nanoen.2019.05.068>.
  135. Jiang, N., and Spence, J.C. (2012). On the dose-rate threshold of beam damage in tem. *Ultramicroscopy* 113, 77–82. <https://doi.org/10.1016/j.ultramic.2011.11.016>.
  136. Egerton, R.F. (2019). Radiation damage to organic and inorganic specimens in the tem. *Micron* 119, 72–87. <https://doi.org/10.1016/j.micron.2019.01.005>.
  137. Shen, B., Wang, H., Xiong, H., Chen, X., Bosch, E.G.T., Lazić, I., Qian, W., and Wei, F. (2022). Atomic imaging of zeolite-confined single molecules by electron microscopy. *Nature* 607, 703–707. <https://doi.org/10.1038/s41586-022-04876-x>.
  138. Li, X., Qiao, J., Chee, S.W., Xu, H.-S., Zhao, X., Choi, H.S., Yu, W., Quek, S.Y., Mirsaidov, U., and Loh, K.P. (2020). Rapid, scalable construction of highly crystalline acylhydrazone two-dimensional covalent organic frameworks via dipole-induced antiparallel stacking. *J. Am. Chem. Soc.* 142, 4932–4943. <https://doi.org/10.1021/jacs.0c00553>.
  139. Taylor, K.A., and Glaeser, R.M. (1976). Electron microscopy of frozen hydrated biological specimens. *J. Ultrastruct. Res.* 55, 448–456. [https://doi.org/10.1016/S0022-5320\(76\)80099-8](https://doi.org/10.1016/S0022-5320(76)80099-8).
  140. Fernandez-Leiro, R., and Scheres, S.H.W. (2016). Unravelling biological macromolecules with cryo-electron microscopy. *Nature* 537, 339–346. <https://doi.org/10.1038/nature19948>.
  141. Liao, M., Cao, E., Julius, D., and Cheng, Y. (2013). Structure of the TrpV1 ion channel determined by electron cryo-microscopy. *Nature* 504, 107–112. <https://doi.org/10.1038/nature12822>.
  142. Li, Y.A., Li, Y.B., Pei, A., Yan, K., Sun, Y.M., Wu, C.L., Joubert, L.M., Chin, R., Koh, A.L., Yi, Y., et al. (2017). Atomic structure of sensitive battery materials and interfaces revealed by cryo-electron microscopy. *Science* 358, 506–510. <https://doi.org/10.1126/science.aam6014>.
  143. Kuwauchi, Y., Yoshida, H., Akita, T., Haruta, M., and Takeda, S. (2012). Intrinsic catalytic structure of gold nanoparticles supported on TiO<sub>2</sub>. *Angew. Chem. Int. Ed. Engl.* 51, 7729–7733. <https://doi.org/10.1002/anie.201201283>.
  144. Tanaka, T., Sano, K., Ando, M., Sumiya, A., Sawada, H., Hosokawa, F., Okunishi, E., Kondo, Y., and Takayanagi, K. (2010). Oxygen-rich Ti<sub>1-x</sub>O<sub>2</sub> pillar growth at a gold nanoparticle-tio<sub>2</sub> contact by O<sub>2</sub> exposure. *Surf. Sci.* 604, L75–L78. <https://doi.org/10.1016/j.susc.2010.09.004>.
  145. Ajayan, P.M., and Marks, L.D. (1989). Evidence for sinking of small particles into substrates and implications for heterogeneous catalysis. *Nature* 338, 139–141. <https://doi.org/10.1038/338139a0>.
  146. Schneider, N.M., Norton, M.M., Mendel, B.J., Grogan, J.M., Ross, F.M., and Bau, H.H. (2014). Electron-water interactions and implications for liquid cell electron microscopy. *J. Phys. Chem. C* 118, 22373–22382. <https://doi.org/10.1021/jp507400n>.
  147. Grogan, J.M., Schneider, N.M., Ross, F.M., and Bau, H.H. (2014). Bubble and pattern formation in liquid induced by an electron beam. *Nano Lett.* 14, 359–364. <https://doi.org/10.1021/nl404169a>.
  148. Roy, P., Lynch, R., and Schmuki, P. (2009). Electron beam induced in-vacuo Ag deposition on TiO<sub>2</sub> from ionic liquids. *Electrochem. Commun.* 11, 1567–1570. <https://doi.org/10.1016/j.elecom.2009.05.051>.
  149. Donev, E.U., Schardein, G., Wright, J.C., and Hastings, J.T. (2011). Substrate effects on the electron-beam-induced deposition of platinum from a liquid precursor. *Nanoscale* 3, 2709–2717. <https://doi.org/10.1039/C1NR10026B>.
  150. den Heijer, M., Shao, I., Radisic, A., Reuter, M.C., and Ross, F.M. (2014). Patterned electrochemical deposition of copper using an electron beam. *Apl. Mater.* 2, 022101. <https://doi.org/10.1063/1.4863596>.
  151. Jeon, S., Heo, T., Hwang, S.Y., Ciston, J., Bustillo, K.C., Reed, B.W., Ham, J., Kang, S., Kim, S., Lim, J., et al. (2021). Reversible disorder-order transitions in atomic crystal nucleation. *Science* 371, 498–503. <https://doi.org/10.1126/science.aaz7555>.
  152. Zewail, A.H. (2010). Four-dimensional electron microscopy. *Science* 328, 187–193. <https://doi.org/10.1126/science.1166135>.
  153. Barwick, B., Park, H.S., Kwon, O.-H., Baskin, J.S., and Zewail, A.H. (2008). 4d imaging of transient structures and morphologies in Ultrafast electron microscopy. *Science* 322, 1227–1231. <https://doi.org/10.1126/science.1164000>.
  154. Fu, X., Chen, B., Tang, J., Hassan, M.T., and Zewail, A.H. (2017). Imaging rotational dynamics of nanoparticles in liquid by 4d electron microscopy. *Science* 355, 494–498. <https://doi.org/10.1126/science.aah3582>.